NASA/TM-2004-213263

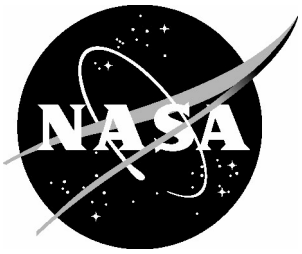

Study and Analyses on the Structural Performance of a Balance

R. Karkehabadi
Lockheed Martin, Hampton, Virginia

R. D. Rhew and D. J. Hope
Langley Research Center, Hampton, Virginia

December 2004

The NASA STI Program Office . . . in Profile

Since its founding, NASA has been dedicated to the advancement of aeronautics and space science. The NASA Scientific and Technical Information (STI) Program Office plays a key part in helping NASA maintain this important role.

The NASA STI Program Office is operated by Langley Research Center, the lead center for NASA's scientific and technical information. The NASA STI Program Office provides access to the NASA STI Database, the largest collection of aeronautical and space science STI in the world. The Program Office is also NASA's institutional mechanism for disseminating the results of its research and development activities. These results are published by NASA in the NASA STI Report Series, which includes the following report types:

- TECHNICAL PUBLICATION. Reports of completed research or a major significant phase of research that present the results of NASA programs and include extensive data or theoretical analysis. Includes compilations of significant scientific and technical data and information deemed to be of continuing reference value. NASA counterpart of peer-reviewed formal professional papers, but having less stringent limitations on manuscript length and extent of graphic presentations.

- TECHNICAL MEMORANDUM. Scientific and technical findings that are preliminary or of specialized interest, e.g., quick release reports, working papers, and bibliographies that contain minimal annotation. Does not contain extensive analysis.

- CONTRACTOR REPORT. Scientific and technical findings by NASA-sponsored contractors and grantees.

- CONFERENCE PUBLICATION. Collected papers from scientific and technical conferences, symposia, seminars, or other meetings sponsored or co-sponsored by NASA.

- SPECIAL PUBLICATION. Scientific, technical, or historical information from NASA programs, projects, and missions, often concerned with subjects having substantial public interest.

- TECHNICAL TRANSLATION. English-language translations of foreign scientific and technical material pertinent to NASA's mission.

Specialized services that complement the STI Program Office's diverse offerings include creating custom thesauri, building customized databases, organizing and publishing research results ... even providing videos.

For more information about the NASA STI Program Office, see the following:

- Access the NASA STI Program Home Page at ***http://www.sti.nasa.gov***

- E-mail your question via the Internet to help@sti.nasa.gov

- Fax your question to the NASA STI Help Desk at (301) 621-0134

- Phone the NASA STI Help Desk at (301) 621-0390

- Write to:
  NASA STI Help Desk
  NASA Center for AeroSpace Information
  7121 Standard Drive
  Hanover, MD 21076-1320

NASA/TM-2004-213263

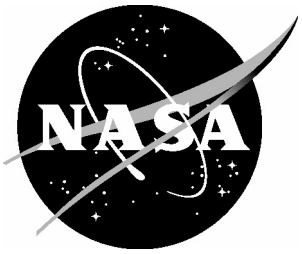

Study and Analyses on the Structural Performance of a Balance

R. Karkehabadi
Lockheed Martin, Hampton, Virginia

R. D. Rhew and D. J. Hope
Langley Research Center, Hampton, Virginia

National Aeronautics and
Space Administration

Langley Research Center
Hampton, Virginia 23681-2199

December 2004

Available from:

NASA Center for AeroSpace Information (CASI)
7121 Standard Drive
Hanover, MD 21076-1320
(301) 621-0390

National Technical Information Service (NTIS)
5285 Port Royal Road
Springfield, VA 22161-2171
(703) 605-6000

Introduction

Strain-gauge balances for use in wind tunnels have been designed at Langley Research Center (LaRC) since its inception. Currently Langley has more than 300 balances available for its researchers. A force balance is inherently a critically stressed component due to the requirements of measurement sensitivity. The strain-gauge balances have been used in Langley's wind tunnels for a wide variety of aerodynamic tests, and the designs encompass a large array of sizes, loads, and environmental effects. There are six degrees of freedom that a balance has to measure. The balance's task to measure these six degrees of freedom has introduced challenging work in transducer development technology areas. As the emphasis increases on improving aerodynamic performance of all types of aircraft and spacecraft, the demand for improved balances is at the forefront.

Force balance stress analysis and acceptance criteria are under review due to LaRC wind tunnel operational safety requirements. This paper presents some of the analyses and research done at LaRC that influence structural integrity of the balances. The analyses are helpful in understanding the overall behavior of existing balances and can be used in the design of new balances to enhance performance. Initially, a maximum load combination was used for a linear structural analysis. When nonlinear effects were encountered, the analysis was extended to include nonlinearities using MSC.Nastran™.

Because most of the balances are designed using Pro/Mechanica®, it is desirable and efficient to use Pro/Mechanica® for stress analysis. However, Pro/Mechanica® is limited to linear analysis. Both Pro/Mechanica® and MSC.Nastran™ are used for analyses in the present work. The structural integrity of balances and the possibility of modifying existing balances to enhance structural integrity are investigated.

Background

A collection of information on topics that may be applicable to balances used in wind tunnels is given here. The topics included are dynamic strength, the effect of rest period on the fatigue life, and residual stress. The balances used in wind tunnels experience cyclic loading. The stress-strain curve of some metals experiencing dynamic loading differs with the stress-strain curve when static loading is applied. The effect of dynamics on the stress-strain curve strength for some materials is shown and discussed.

Important and possibly applicable to wind tunnel balances is the effect of the rest period on fatigue life. The fatigue resistance of a material is usually based on data obtained from an uninterrupted fatigue test. The balances are not used uninterrupted until failure; consequently, the influence of rest periods on the fatigue life needs to be investigated. Also, the effect of periodic overloading and residual stresses is discussed briefly. The results shown here may not be from the same material and/or same condition as the wind tunnel balances; however, the discussion gives insight on how these factors may influence the structural integrity of the balances.

High-Strain-Rate Mechanical Response

The mechanical response of metals under high rates of loading may differ significantly from the corresponding response within the static regime. Kolsky (ref. 1) shows a comparison between the "dynamic" stress-strain curve for annealed bars of aluminum and the "static" stress-strain curve for similar bars (fig. 1). The effect of the strain-rate is obvious in this figure. Haddad (ref. 2) also gives this figure in his research.

Figure 2 plots compressive stress-strain curves for the alloy Ti-6% Al-4% from Meyers (ref. 3). For Ti alloys, a considerable strain-rate strengthening is observed. Figure 3 shows the stress-strain response for commercially pure Ti (from ref. 4). The gradual increase in flow stress as the strain-rate increases is obvious. Haddad reports that some metals, such as aluminum and copper, may not show sensitivity to both strain-rate and strain-rate history. Other metals, such as steel and titanium, show sensitivity to strain-rate only.

Hopkinson (ref. 5) conducted a series of dynamic experiments on steel and concluded that the dynamic strength was at least twice as high as its low-strain-rate strength. It is also known that steel undergoes a ductile-to-brittle transition when the strain-rate is increased. Therefore, it is normal to be curious about the effect of strain-rate on the strength of materials.

Increase in Fatigue Life Caused by Rest Periods

The fatigue resistance of a material is usually based on data derived from an uninterrupted fatigue test. In practice, it is rare that loads are applied without any rest period. The condition of the rest period applies to balances used in wind tunnels. What then is the effect of the rest period on fatigue endurance?

In a paper by Miller and Hatter (ref. 6), due to the inclusion of rest periods, an unusual increase in fatigue resistance of steel alloys is reported. Based on this test, it is reported that the introduction of rest periods always causes an increase in endurance, which approaches a maximum of approximately 100 percent at a critical value of rest. The total rest period is a more important parameter than either the number of rest periods or the position in the lifetime at which rests may be taken. As indicated in figure 4, after a rest period of 100 hours, the maximum increase of endurance is about 100 percent. Thereafter, the improvement in endurance is reduced, and with a rest period of 200 hours the increase in endurance is approximately constant at 33 percent.

During the rest periods, the specimens are still subject to high residual stresses. The highly deformed and still highly stressed zones at crack tips could undergo a relaxation of stress due to dislocation mobility. This effect could cause recovery and the crack-tip material to be in a lower cyclic stress-strain state after a rest period, with a consequent decrease in crack growth rate and an increase in endurance (ref. 7).

Overloading and Effects of Residual Stresses

It is widely recognized that the main factor dominating the initiation and propagation of cracks is cyclic plasticity at stress concentrations. More information and references are provided by Watson, Hoddinott, and Norman and are available in *American Society for Testing and Materials* (ASTM), or reference 8. The cyclic stress-strain curve for a complex varying load differs from that in a constant amplitude test.

Several investigations have shown preloading and periodic overloading can increase fatigue resistance under variable amplitude conditions (ref. 9). His explanation of these results is based on stress interaction effects and on the induction of compressive residual stresses near the crack tip. If the overloads were compressive, a decrease in life would be expected. Jacoby (ref. 10) reports a life reduction of about 45 percent. In reference 8, periodic overloads and random fatigue behavior are investigated. This paper reports that in the absence of residual stresses, periodic high overstrains make a major contribution to fatigue damage.

Stress Analysis

Balance 1621 is typical for Langley Research Center (LaRC) designed balances and was chosen for this study due to its traditional high load capacity. Maximum loading occurs when all six components are applied simultaneously with their maximum allowables (limit loads). This circumstance normally will not occur during wind tunnel testing; however, if it occurs, is the balance capable of handling the loads with an acceptable margin of safety? Preliminary analysis using Pro/Mechanica® indicated that this balance might experience nonlinearity. It was decided to analyze this balance using MSC.Nastran™ so that a nonlinear analysis could be conducted.

Balance 1621 was modeled and meshed in MSC.Patran™ for analysis in MSC.Nastran™. The model from Patran/Nastran is compared with that from Pro/Mechanica®. For a complete analysis, it is necessary to consider all the load cases as well as use a dense mesh near all the edges. Because of computer limitations, it is not possible to have one model with the dense mesh near all edges. In the present study, the dense mesh is limited to the surface on the end of the axial sections.

Four different load combinations are used in the current analysis. Linear analysis is performed for each load case. When the stress value is above the linear elastic region, it is necessary to perform a nonlinear analysis. Two load combinations, those used here, are examples where stresses are above the linear region and require nonlinear analysis. Not all load combinations result in stresses above yield, and two such load combinations are also selected for analysis.

Applied Load

The limit loads for the balance were obtained from the NASA Balance 1621 (ref. 11) drawing and are listed in table 1. The loads are in the coordinate system shown in figure 5.

Four different load combinations are considered.

Case 1:

$\vec{F}_x = -500\ \hat{i}$

$\vec{F}_y = 1800\ \hat{j}$

$\vec{F}_z = -3000\ \hat{k}$

$\vec{M}_o = 7500\hat{i} + 10000\,\hat{j} + 4500\ \hat{k}$

Case 2:

$\vec{F}_x = -500\ \hat{i}$

$\vec{F}_y = 1800\ \hat{j}$

$\vec{F}_z = 3000\ \hat{k}$

$\vec{M}_o = 7500\ \hat{i} - 10000\ \hat{j} + 4500\ \hat{k}$

Case 3:

$\vec{F}_x = -500\ \hat{i}$

$\vec{F}_y = 1800\ \hat{j}$

$\vec{F}_z = -3000\ \hat{k}$

$\vec{M}_o = -7500\ \hat{i} + 10000\ \hat{j} + 4500\ \hat{k}$

Case 4:

$\vec{F}_x = -500\ \hat{i}$

$\vec{F}_y = 1800\ \hat{j}$

$\vec{F}_z = 3000\ \hat{k}$

$\vec{M}_o = -7500\ \hat{i} - 10000\,\hat{j} + 4500\ \hat{k}$

The values given are valid when applied at moment center, o. The loads are applied at point p, hence transformation is required. The transformation of the loads from moment center (MC) to point p is done using equation (1):

$$\vec{M}_p = \vec{R}_{po} \times \vec{F} + \vec{M}_o = 4.1\,\hat{i} \times \left(\vec{F}_x + \vec{F}_y + \vec{F}_z\right) + \vec{M}_o \tag{1}$$

Table 1. Maximum Forces and Moments (Limit Loads)
for Balance 1621

Force and moment components	Force (lb) and moment (in-lb) values
Axial, F_x	500
Side, F_y	1800
Normal, F_z	3000
Roll, M_x	7500
Pitch, M_y	10000
Yaw, M_z	4500

Moment components for each case are obtained after substituting into equation (1):

$\vec{M}_p = 7500\ \hat{i} + 22300\ \hat{j} + 11880\ \hat{k}$ for case 1

$\vec{M}_p = 7500\ \hat{i} - 22300\ \hat{j} + 11880\ \hat{k}$ for case 2

$\vec{M}_p = -7500\ \hat{i} + 22300\ \hat{j} + 11880\ \hat{k}$ for case 3

$\vec{M}_p = -7500\ \hat{i} - 22300\ \hat{j} + 11880\ \hat{k}$ for case 4

Material Property

The properties used in the present work for linear stress analysis are from the Teledyne Vasco catalog and shown below:

E = 27550 ksi (Young's modulus of elasticity)
ν = 0.31 (Poisson's ratio)

The stress-strain curve used for nonlinear analysis is obtained from the Department of Defense (ref. 12) and is shown in figure 6.

Modal Analysis

In order to better understand the structural behavior of this balance and compare models from MSC.Patran™ with those from Pro/Engineer®, a modal analysis was performed. The natural frequencies and mode shapes were obtained from Pro/Mechanica® and MSC.Nastran™. Single-pass adaptive (SPA) analysis was used in obtaining the results from Pro/Mechanica®. The first three frequencies from both Pro/Mechanica® and MSC.Nastran™ are given in table 2.

Table 2. Frequencies From MSC.Nastran™ and Pro/Mechanica®

Mode	Frequency, Hz Pro/Mechanica®	Frequency, Hz MSC.Nastran™	Mode shape
1	335.3	344.42	Bending about Z-axis
2	341.9	350.65	Bending about Y-axis
3	1066	1225.5	Axial

The mode shapes obtained from Pro/Mechanica® are shown in figures 7, 8, and 9. The first two modes are bending about the Z- and Y-axes, respectively. The third mode is axial, in X direction. Figures 10, 11, and 12 are the first three mode shapes of the balance from MSC.Nastran™ results. These results follow the same trend as those from Pro/Mechanica®. The first mode is bending about the Z-axis, the second mode is bending about the Y-axis, and the third mode is axial. The comparison of the mode shapes and frequencies from MSC.Nastran™ with Pro/Mechanica® indicates that the two models are similar.

Linear Analysis

The present model was generated and meshed using MSC.Patran™. The section of the material where the load was applied is not modeled in order to reduce the number of elements. The load is applied at point p and transferred to the balance through a rigid element. One load case that produces regions of high stress on the balance, load case 1, is used here. This load case has all positive components except axial force (F_x) and normal force (F_z). The components of the load applied at point p are shown in the load section. The results are expected to be accurate away from the applied load due to St. Venant's principle.

Global Analysis

Because of computer limitations, the model was meshed using about 200000 elements: all 10-node tetrahedral elements, or tet10. The result of this run is used for global-local analysis. The whole balance is first analyzed as a global entity; discarding details does not affect the overall behavior. Local details are then analyzed using the results of the global analysis. With this method the detail analysis is done on the selected regions. Through detail analysis of selected regions computational time is saved. A three-dimensional view of the meshed model used in the present work is shown in figure 13.

The von Mises stress and principal stresses for the axial section near the applied load are shown in figures 14 and 15. Maximum von Mises stress (267 ksi) and principal stress (274 ksi) both occur on the axial section. The values shown are for the coarse mesh, and to find more accurate results more elements are needed, particularly near the corners.

Local Analysis of Axial Section

There are many corners on the balance and, in order to capture the stress gradient, a dense mesh is required near these corners. In order to use more elements, and because of computer limitations, the global model has to be divided into smaller local sections. A section near the applied load was extracted and meshed (fig. 16). The results of the global model were used as the boundary condition for this local model. The von Mises and principal stresses are shown in figures 17 and 18. As the results indicate, the maximum stress values are above yield stress, indicating that nonlinear analysis is needed.

Model for Nonlinear Analysis

Results from the linear analysis indicate that the stress value is above the linear elastic region; hence, nonlinear analysis is required. Both geometrical and material nonlinearities are considered here. The model used for nonlinear analysis is meshed with 4-node tetrahedral elements, or tet4. The balance is meshed with almost 400000 tet4 elements (fig. 19). More elements are used near sharp corners. A dense mesh is used near the end of the axial sections (fig. 20). Linear analysis was performed on the balance with the new mesh and all four load cases were considered. When the linear analysis indicates a maximum stress value below yield stress, nonlinear analysis was not performed.

Case 1: Loading

The full model is used for the linear and nonlinear analysis. A local model used in the linear analysis is used here again for comparison.

Global Model

Results of the analysis for the load combination of case 1 are given subsequently. The full model is used and the results from the linear and nonlinear analyses are shown.

Linear Analysis. Von Mises stress from the linear analysis for the balance is given in figure 21. As the figure indicates, the maximum stress occurs at the end of the axial section and is above the ultimate stress.

Nonlinear Analysis. Von Mises stress from the nonlinear analysis for the balance is given in figure 22. As expected, the value of the maximum von Mises stress dropped in comparison with the linear case.

In order to have an overall view of the stresses everywhere on the balance, figure 23 is plotted and illustrates the position versus von Mises stress for all points on the balance. The figure clearly indicates that there are high stress regions. The maximum stress values are localized and peak stresses occur at the end of the axial sections. It should be noted that the maximum stress value near other corners might increase as more dense mesh is used near those corners. However, in the present work, the interest is at the end of the axial section.

Stress values on the +Y and −Y sides of the balance are plotted individually and shown in figures 24 and 25. As shown, the maximum stress occurs on the −Y side of the balance for this load case.

Local Model

The local model of the balance used for the linear analysis is used here again for global-local analysis. The local model is meshed with tet4 elements for the nonlinear analysis (fig. 26) and the boundary conditions are obtained from the linear run. The von Mises and principal stresses for the nonlinear analysis are given in figures 27 and 28. The comparison of the linear and the nonlinear runs for the axial section close to the applied load is shown in table 3. As expected, stresses obtained from the nonlinear analysis dropped in comparison with the linear analysis and are in agreement with the analysis of the global model.

Table 3. Maximum von Mises and Principal Stresses From Local Model

Stress	Linear analysis, ksi	Nonlinear analysis, ksi
Von Mises	351	287
Principal	312	249

Case 2: Loading

Linear Analysis

The von Mises stress from the linear analysis for the balance is shown in figures 29 and 30. As indicated, the high stress occurs at the end of the axial section.

Nonlinear Analysis

The von Mises and principal stresses from the nonlinear analysis are shown in figures 31 and 32. As expected, the maximum stress value for the von Mises and principal stresses dropped in comparison with the linear analysis.

In order to have an overall view of the stresses everywhere on the balance for this load case, figures 33 and 34 are plotted. Figure 33 is a plot of the stress for the von Mises, and figure 34 is a plot of the principal stress on the balance.

Cases 3 and 4: Loading

Results of the analyses for load cases 3 and 4 demonstrate that because the value of stress for both cases is below yield, nonlinear analysis was not required. These two load cases are examples of the cases that produce stresses below yield.

Linear Analysis

Figures 35 and 36 are the von Mises and principal stresses from the linear analysis for load case 3. Figures 37 and 38 are the results from load case 4. The von Mises stress from the linear analysis for the balance is shown in figure 37, and the principal stress is shown in figure 38. As the figures indicate, the stresses are below yield.

Discussion

Modal analysis was performed to compare the models from Pro/Engineer® and MSC.Patran™. Linear and nonlinear analyses were performed with different load combinations. Four different load combinations were used and two of the load combinations required nonlinear analysis. Maximum loads were used in the present analysis. Maximum loading occurs when all six components are applied simultaneously with their maximum allowables, a circumstance that normally does not occur during wind tunnel testing. As table 4 indicates, the nonlinear results for the von Mises stresses are below yield.

Table 4. Linear and Nonlinear Analysis

Case	Linear analysis—von Mises, ksi	Linear analysis—principal, ksi	Nonlinear analysis—von Mises, ksi
1	361		278
2	343	367	282
3	215	233	
4	237	253	

Design Modification and Analyses of Existing Balance

In the present section, some of the regions where highly localized stress occurs are modified. Figures 39 and 40 show the balance with its coordinate system. Some of the high stress regions of interest are numbered and shown in these figures. Locations 1, 2, 3, and 4 are among the regions where maximum stresses occur. In order to increase the fillet size at the outer regions of locations 1 through 4, a cut was

made followed by a fillet radius of 0.05 in. Figure 41 shows the closeup view before and after modification of the balance at location 4.

The potential impact of design modifications should be mentioned. Design modifications to existing balances such as increased fillet sizes can potentially impact performance. The fillets will decrease bulkhead stiffness, which will lead to additional deflection. This additional deflection may lead to a decrease in sensitivities and an increase in interactions. Both factors will degrade balance accuracy.

Results

In order to investigate the effect of each component of force on the balance, the maximum von Mises stress due to each individual component is shown in table 5. Locations 1 through 4 and T-sections are monitored for each load component. The table shows von Mises stresses due to F_y, M_x, and M_z at the four locations and von Mises stresses at T-sections due to F_z and M_y. Also, the maximum von Mises stress and the location where this maximum occurs is shown in the table. The stress values are given for the model before and after modification.

Table 5. Maximum von Mises Stress Before and After Modification for Each Load Component

Model	Location	F_x	F_y	F_z	M_x	M_y	M_z
Before modification, ksi	1, 2, 3, or 4		71		240		160
	T-section			100		200	
	Maximum value [Location of maximum stress]	50 [10]	86 [11]	240 [11]	240 [3]	250 [11]	160 [2,3]
After modification, ksi	1, 2, 3, or 4		51		200		120
	T-section			66		140	
	Maximum value [Location of maximum stress]	50 [10]	70 [11]	150 [11]	200 [1]	160 [11]	150 [Behind the second cut on location 3]

Next, one of the load combinations is considered: −Fx, −Fy, Fz, Mx, −My, and −Mz. The Pro/Mechanica® results show that this load combination results in high stress near region 4. As shown in table 6, the maximum von Mises stress before modification was 450 ksi and after modification dropped to 350 ksi. Up to this point the analysis was done using single-pass adaptive (SPA). To obtain more accurate results, the analysis was continued using multipass adaptive (MPA). Convergence for local displacement, local strain energy, and global rms stress was set to 7 percent. Due to computer limitations, the specified convergence was not achieved. The results in table 6 are for the convergence of 10 percent.

Table 6. Maximum von Mises Stress Before and After Modification for Load Combination $-F_x$, $-F_y$, F_z, M_x, $-M_y$, and $-M_z$ With 10-Percent Convergence

Method	Before modification, ksi	After modification, ksi
SPA	450	350
MPA	430	360

Figures 42 and 43 show the maximum von Mises stresses, using MPA, before and after modification. The maximum stress occurs at location 4 for both cases.

Enhancing the Structural Integrity of Existing Balance

In the previous section, the balance was slightly modified and analyzed. The analysis was done using Pro/Mechanica®. The balance was also modified in MSC.Patran™ and analyzed using MSC.Nastran™ by Karkehabadi (ref. 13). The analyses on the modified balance indicate a reduction of the maximum von Mises stress for the load case applied. The result obtained from the modified balance, shown previously, is encouraging. Consequently, it was decided to further modify the same balance in order to further reduce the maximum stress values near the sharp corners. In the present section, further modifications are added to the regions where high stresses occur, and new analyses are performed.

In the revised model, the fillet sizes of the sharp corners are increased. This modified balance is referred to as model B, shown in figure 44. In order to increase the fillet sizes, some material is extracted from the balance. The previous modification, shown earlier, is referred to as model A.

Results

The maximum von Mises stress due to five individual components is shown in table 7. F_x is not included because its value is small and does not contribute significantly on the stress near the regions of interest. High stress regions, locations 1 through 4 and T-sections, are monitored for each load component. The table shows von Mises stresses due to F_y, M_x, and M_z at locations 1 through 4 and von Mises stresses at T-sections due to F_z and M_y.

Table 7. Maximum von Mises Stress Before and After Modifications for Five Individual Load Components

Model	Location	F_y	F_z	M_x	M_y	M_z
Before modification, ksi	1, 2, 3, or 4	71		240		160
	T-section		100		200	
After modification A, ksi	1, 2, 3, or 4	51		200		120
	T-section		66		140	
After modification B, ksi	1, 2, 3, or 4	31		107		59
	T-section		46		98	

One load combination that produces high stresses in regions 1 through 4 is used here, $-F_x$, $-F_y$, F_z, M_x, $-M_y$, and $-M_z$. The Pro/Mechanica® analysis shows that this load combination produces high stress near region 4. As shown in table 8, the maximum von Mises stress before modification was 450 ksi, after modification it dropped to 350 ksi for model A and 267 ksi for model B. Up to this point the analysis was done using SPA. To obtain more accurate results, the analysis was continued using MPA. Convergence for local displacement, local strain energy, and global RMS stress was set to 7 percent. Due to computer limitations, the specified convergence was not achieved. The results given in table 8 are for the convergence of 10 percent.

Figure 42 shows the maximum von Mises stress, using MPA, before modification. Figure 45 shows the maximum von Mises stresses for model B.

Table 8. Maximum von Mises Stress Before and After Modification for Load Combination $-F_x$, $-F_y$, F_z, M_x, $-M_y$, and $-M_z$ on Models A and B

Method	Before modification, ksi	After modification, model A, ksi	After modification, model B, ksi
SPA	450	350	267
MPA	430	360	250

Concluding Remarks

Based on the studied experiment(s) on steel, the dynamic strength is known to be at least twice its low-strain-rate strength. There is a strong possibility that the strength of some balances experiencing cyclic loading is greater than the strength derived from a static stress-strain curve. The fatigue resistance of a material is usually based on data derived from the uninterrupted fatigue test. Because the balances are not used uninterrupted until failure, an increase in the fatigue life is expected. Linear analysis for some load combinations indicates stresses above ultimate. Because the stress is above the linear elastic region, a nonlinear analysis was performed. The maximum von Mises stress from the nonlinear analysis is in the vicinity of the yield stress and it does not satisfy the factor of safety required. Factors affecting the structural integrity of the balances, such as dynamic loading, increase in fatigue life caused by rest period, and overloading were investigated. Most of these factors help to enhance the structural integrity of the balances.

Not all the balances and not all the load combinations need nonlinear analysis. Pro/Mechanica®, MSC.Nastran™, or other finite element software can be used for linear analysis of the existing balances. For a complete analysis, all the load cases need to be considered. Having the model in Pro/Engineering® makes Pro/Mechanica® a good candidate for stress analysis. If the maximum stress value obtained is beyond yield, either a change in the design is needed or the maximum loads allowed need to be reduced. The reduction of the force in certain components is practical because, in most cases, the wind tunnel tests do not require maximum value of the loads on all components. In some cases, the wind tunnel test may require some components above their maximum values whereas the maximum values of the other components are not needed and can be reduced.

For the balances that will be designed in the future, it is important to consider the factor of safety in the design stage. Increasing the size of the fillets helps to relieve some of the high stresses, which occur locally. In some locations, such as the end of the axial section, the sharpness on one side can be removed by taking the unnecessary sharp corners out. This can be done on the new or existing balances. Doing so will reduce the maximum value of stress from those corners with little effect on the overall performance of the structure.

In order to reduce the stress value near the sharp corners, the balance was modified. Modifications were made to the balance in order to increase the fillet sizes. One load combination that produces high stress at location 4 was used. The analysis indicates a lower stress value near the sharp corners after modification. Not all of the load combinations were used here. However, the results from the load case analyzed indicate that there is a possibility of enhancing the structural integrity of balances by modifying and increasing fillet size on sharp corners. The potential impact of design modifications should be mentioned. Design modifications to existing balances, such as increased fillet sizes, can increase structural integrity of balances.

References

1. Kolsky, H.: The Propagation of Stress Pulses in Linear Viscoelastic Solids. *Philosophical Magazine* 1, 1965, pp. 693–711.

2. Haddad, Y. M.: *Mechanical Behaviour of Engineering Materials*. Kluwer Academic Publishers, 2000.

3. Meyers, M. A.: *Dynamic Behavior of Materials*. John Wiley & Sons, Inc., 1994.

4. Meyers, M. A.; Subhash, G.; Kad, B. K.; and Prasad, L.: Evolution of a Microstructure and Shear-Band Formation in a α-hep Titanium. *Mechanics of Materials*, 17, 175, 1994.

5. Hopkinson, B.: Effects of Momentary Stresses in Metals. *Proc. Roy. Soc.*, vol. A74, 1905, pp. 498–506.

6. Miller, K. J.; and Hatter, D. J.: Increase in Fatigue Life Caused by the Introduction of Rest Periods. *J. Strain Analysis*, vol. 7, 1972, pp. 69–73.

7. Tomkins, B.: Low Cycle Fatigue in Metals and Polymers. Thesis, University of Cambridge, 1965.

8. Watson, P.; Hoddinott, D. S.; and Norman, J. P.: Periodic Overloads and Random Fatigue Behavior. Paper presented at *Cyclic Stress-Strain Behavior-Analysis, Experimentation, and Failure Prediction Symposium*, ASTM, Philadelphia, PA, 1971.

9. Schijve, J.; Cumulative Damage Problems in Aircraft Structures and Materials. *The 11th Conference of the International Committee on Aeronautic Fatigue*, 1969.

10. Jacoby, G. H.: *Fatigue Life Estimation Processes Under Conditions of Irregularly Varying Loads*. Tech. Rep. AFML-TR-67-215, Air Force Materials Laboratory, Aug. 1967.

11. Balance 1621 Drawing, LD-931502.

12. Department of Defense: *Metallic Materials and Elements for Aerospace Vehicle Structures*. MIL-HDBK-5H, 1998.

13. Karkehabadi, R.: *Analysis on a Modified Existing Balance Using PATRAN/NASTRAN*. Lockheed Martin Report SDSR- 43RB0-050903, May 2003.

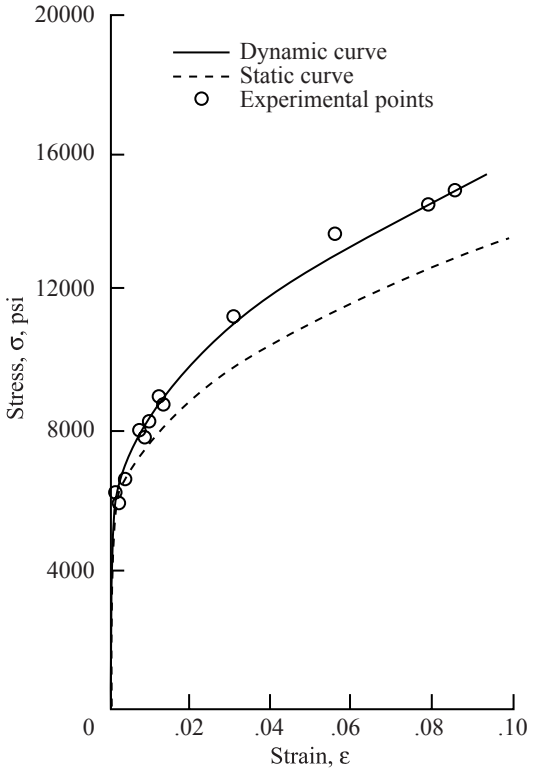

Figure 1. Dynamic and static stress-strain curves for annealed aluminum.

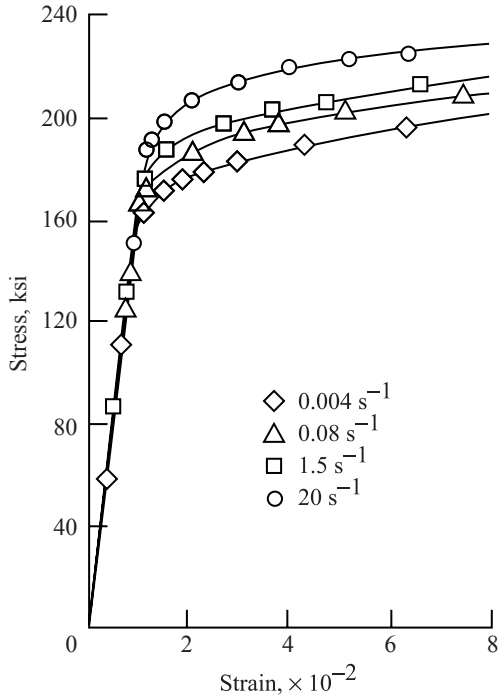

Figure 2. Effect of strain-rate on stress-strain response (in compression) of Ti-6% Al-4% alloy.

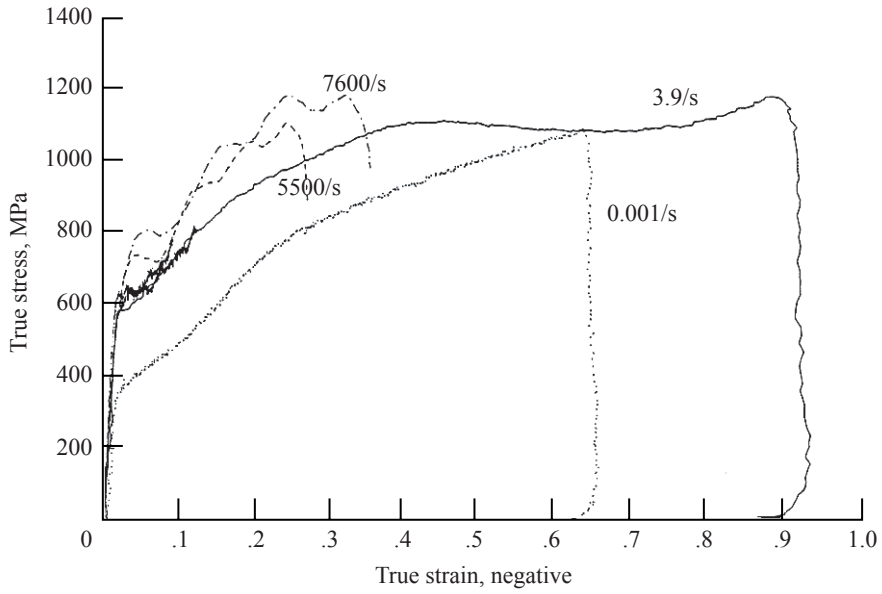

Figure 3. Effect of strain-rate on stress-strain response (in compression) of commercially pure Ti.

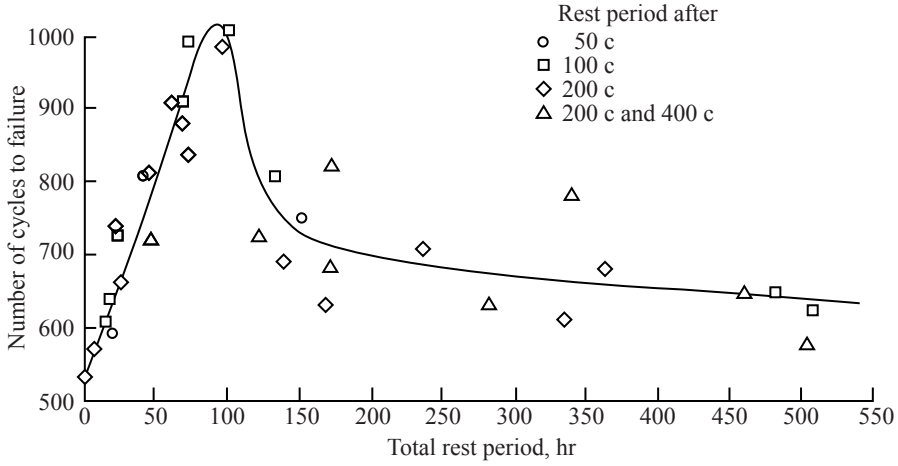

Figure 4. Effect of duration of rest periods on fatigue endurance.

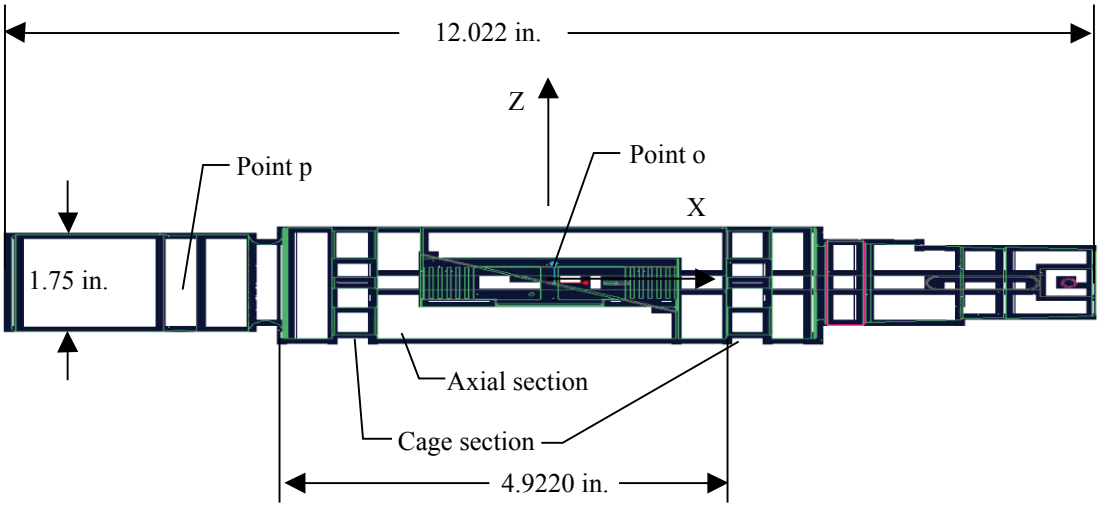

Figure 5. Balance 1621 with coordinate axis located at moment center.

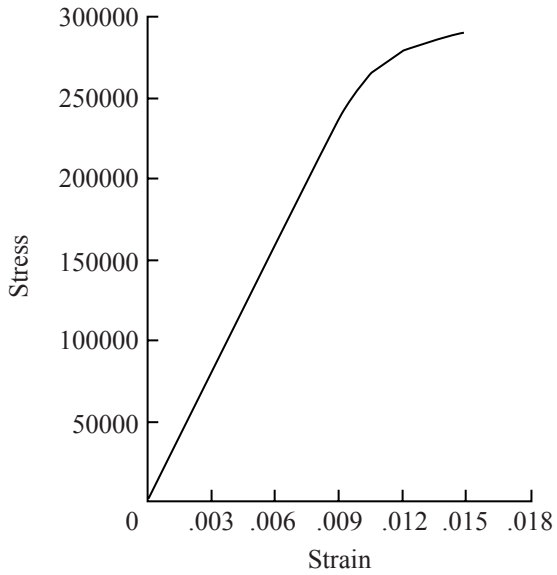

Figure 6. Tensile stress-strain curve at room temperatures for 280 maraging steel bar.

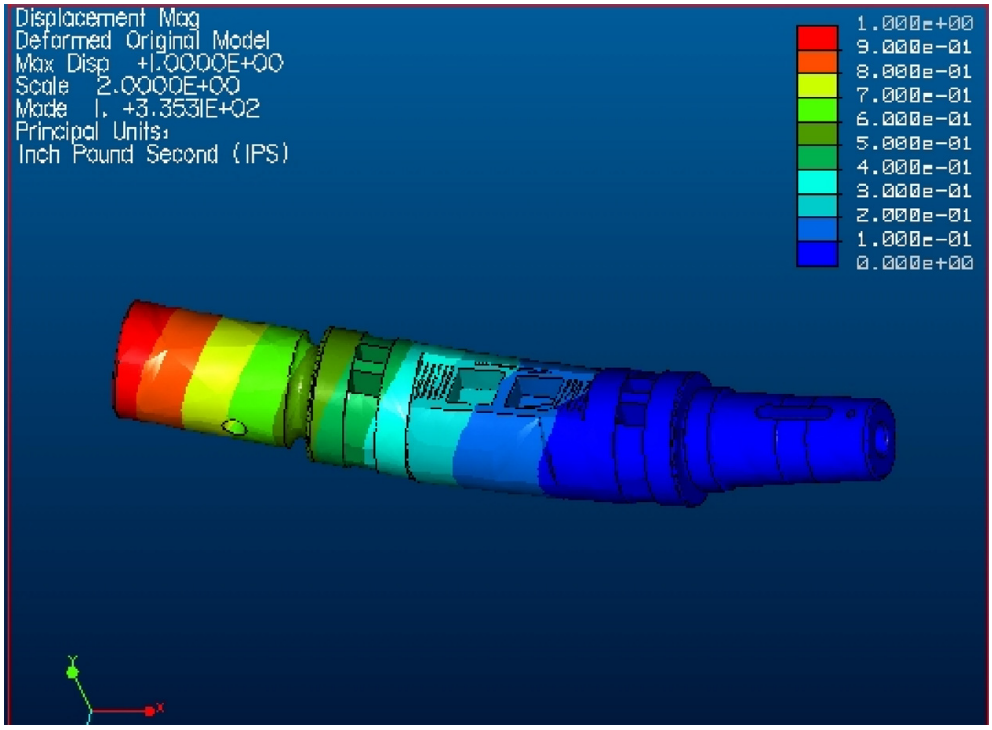

Figure 7. First mode shape using results from Pro/Mechanica®, bending about Z-axis.

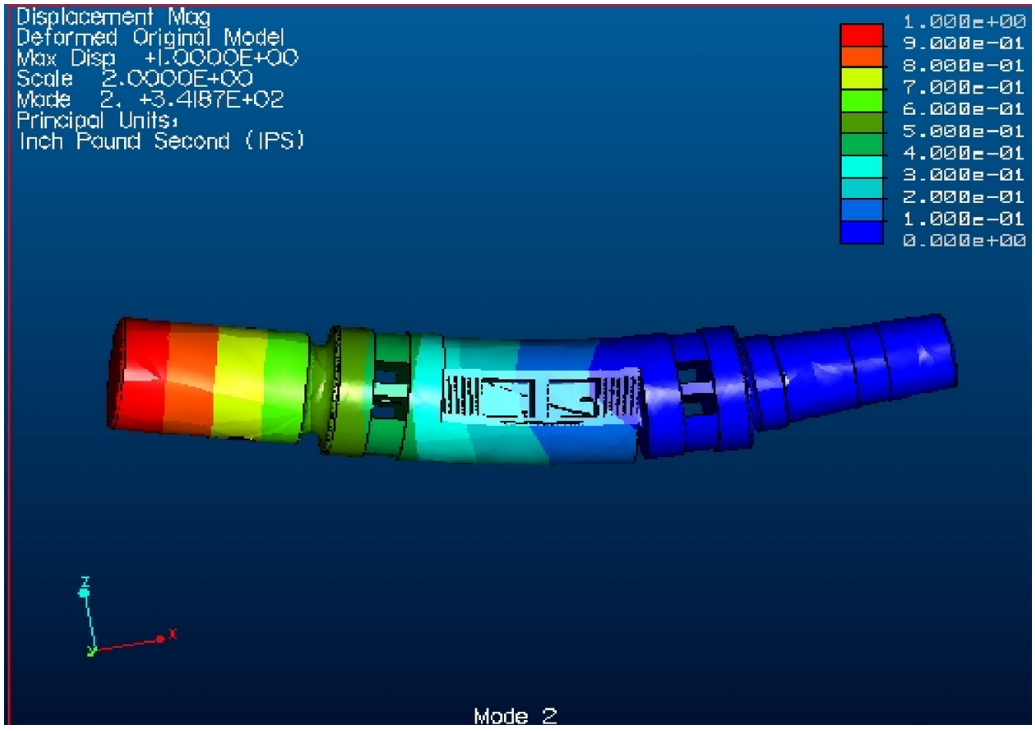

Figure 8. Second mode shape using results from Pro/Mechanica®, bending about Y-axis.

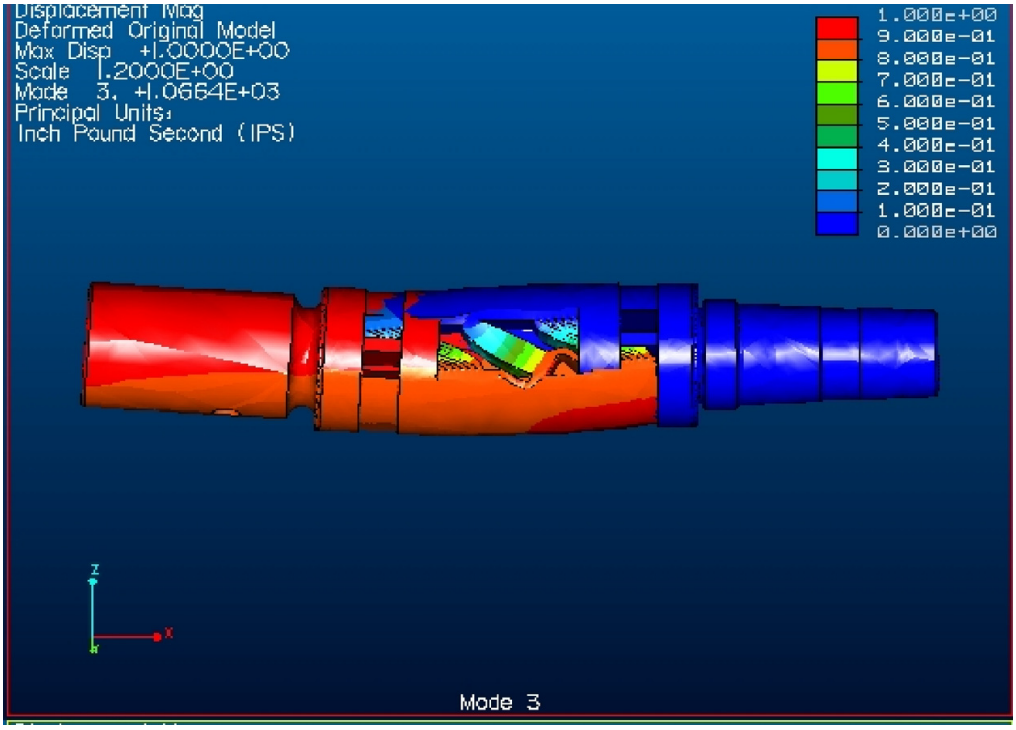

Figure 9. Third mode shape using results from Pro/Mechanica®, axial.

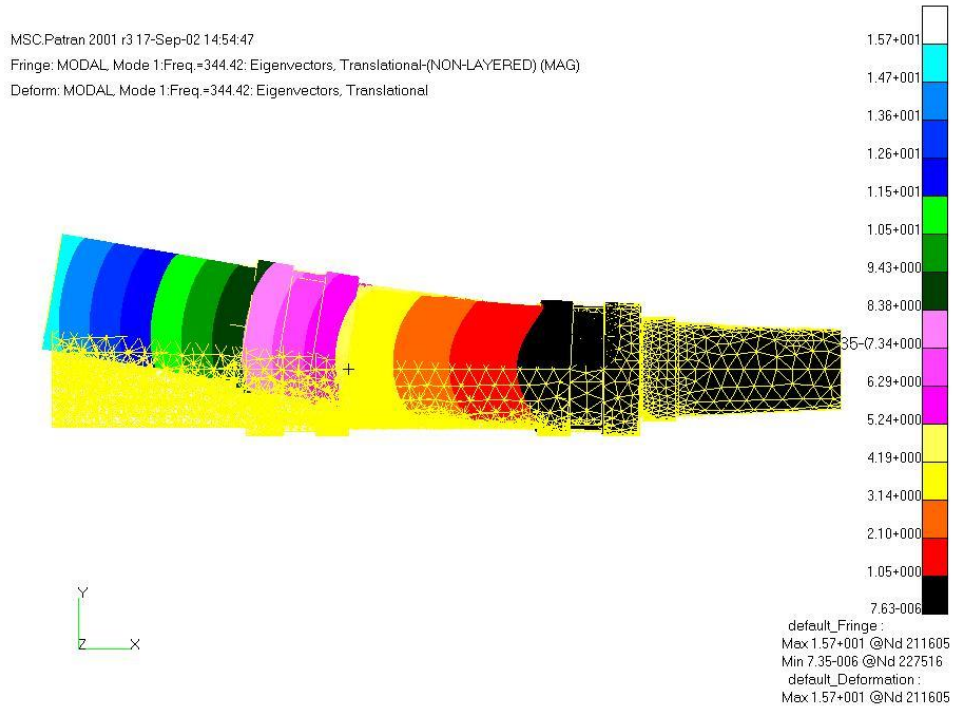

Figure 10. First mode shape using results from MSC.Nastran™, bending about Z-axis.

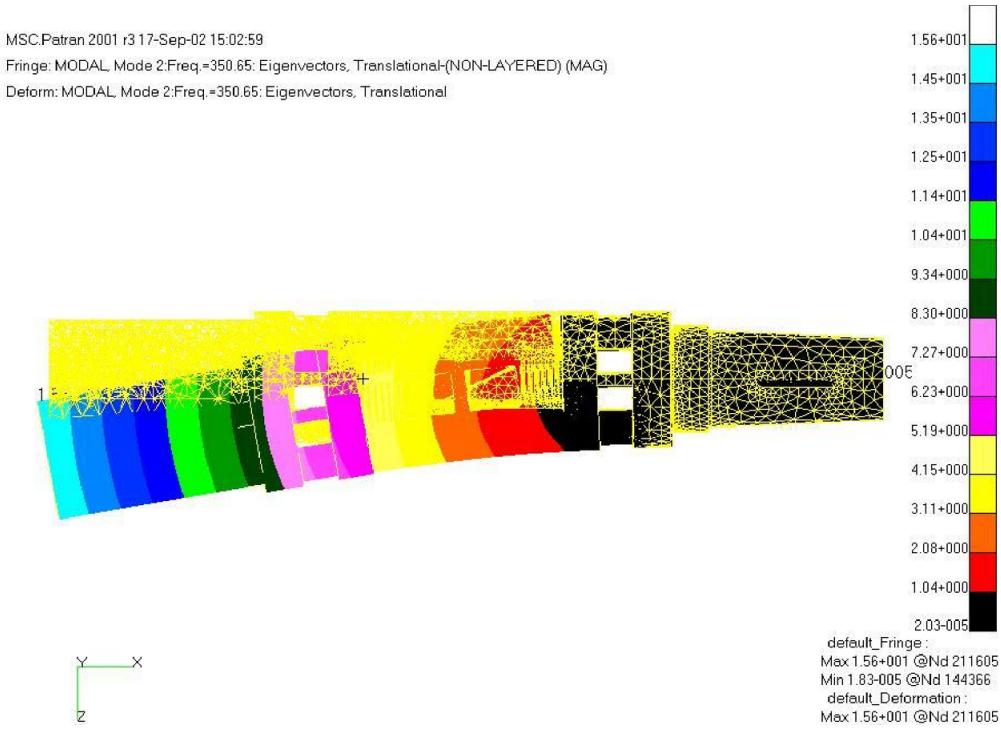

Figure 11. Second mode shape using results from MSC.Nastran™, bending about Y-axis.

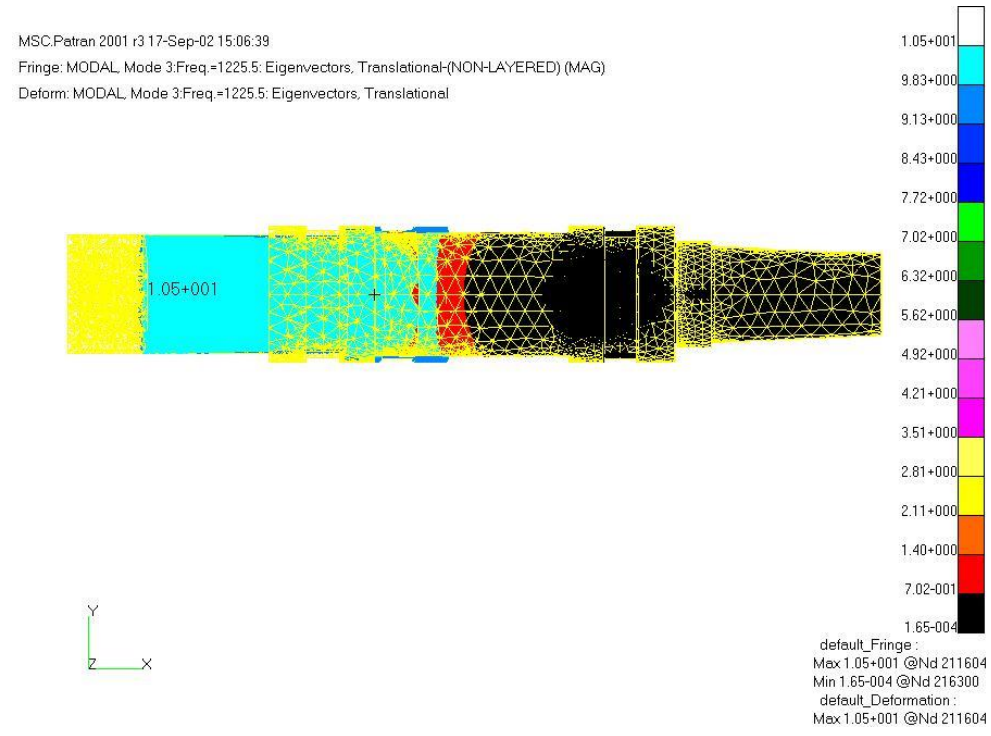

Figure 12. Third mode shape using results from MSC.Nastran™, axial.

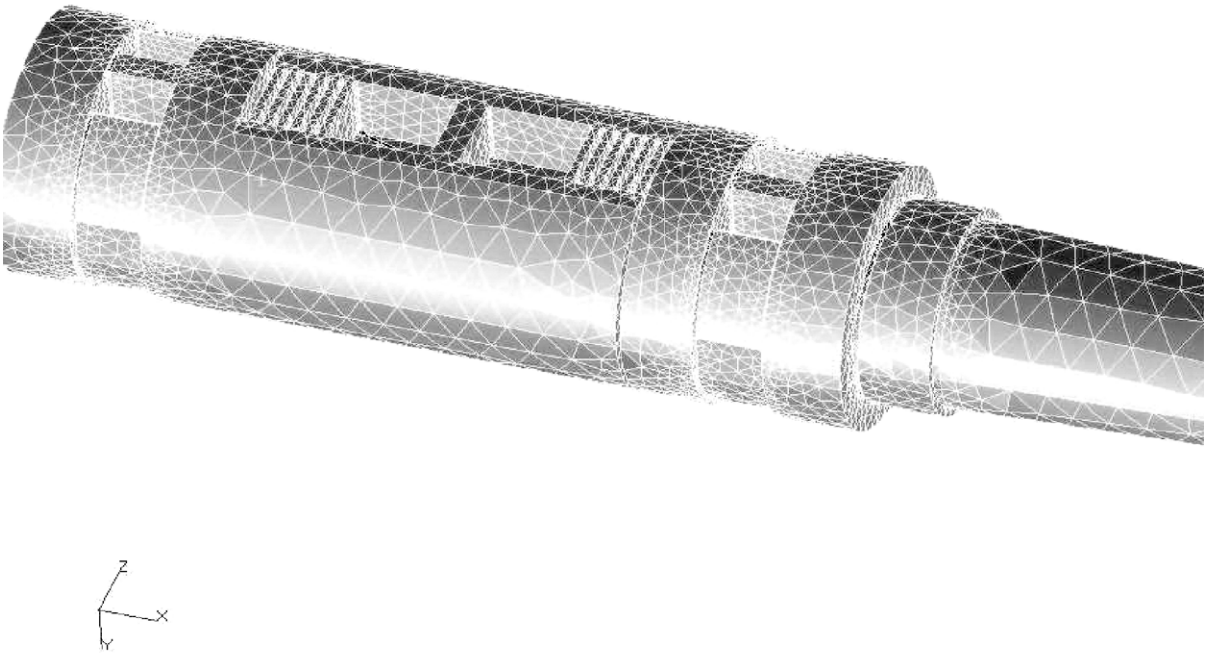

Figure 13. A 3-D view of balance modeled and meshed in MSC.Patran™.

Figure 14. Von Mises stress for balance, load case 1.

Figure 15. Maximum principal stress for balance, load case 1.

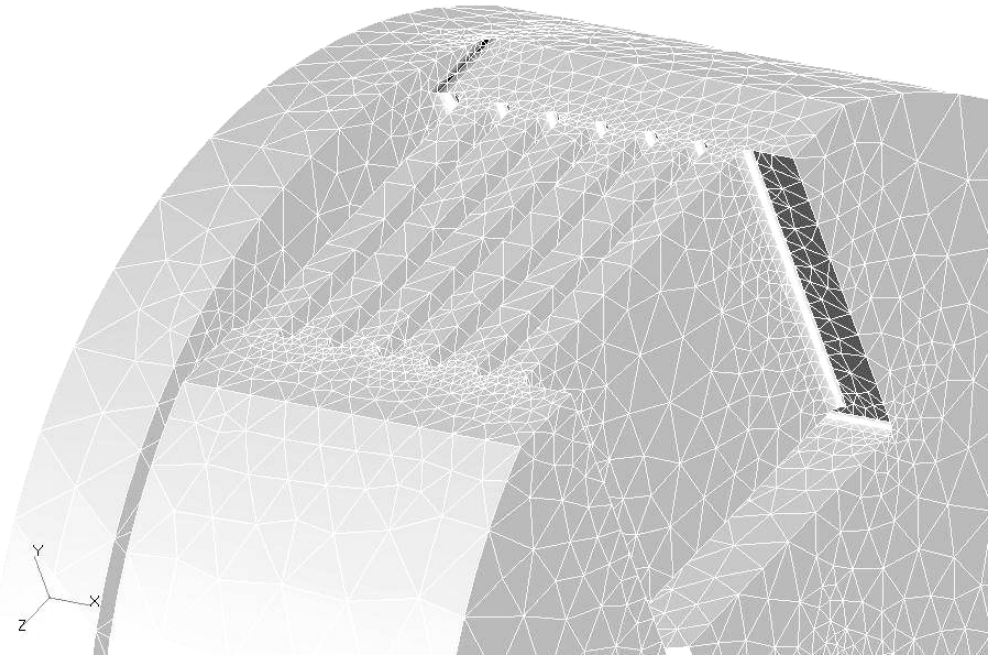

Figure 16. Meshed view of balance section near applied load.

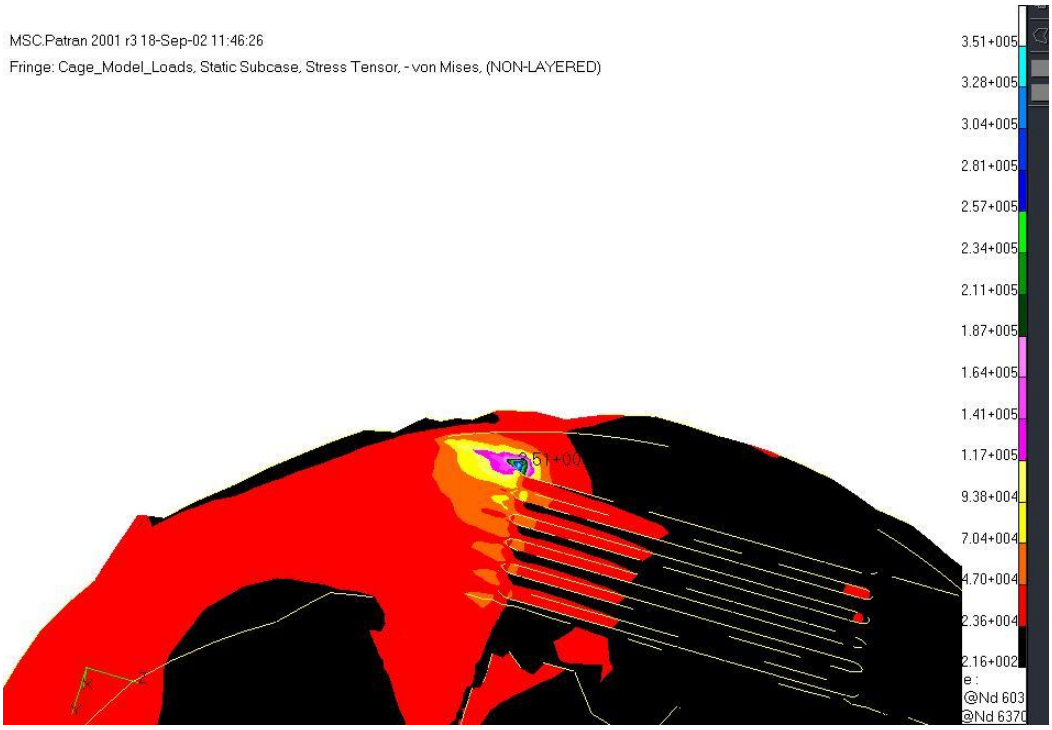

Figure 17. Von Mises stress for balance section near applied load.

Figure 18. Principal stress for balance section near applied load.

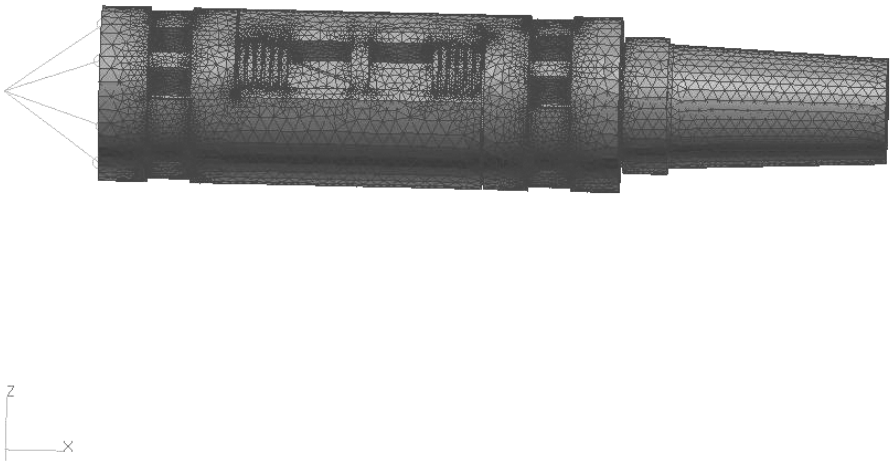

Figure 19. Meshed balance for nonlinear analysis.

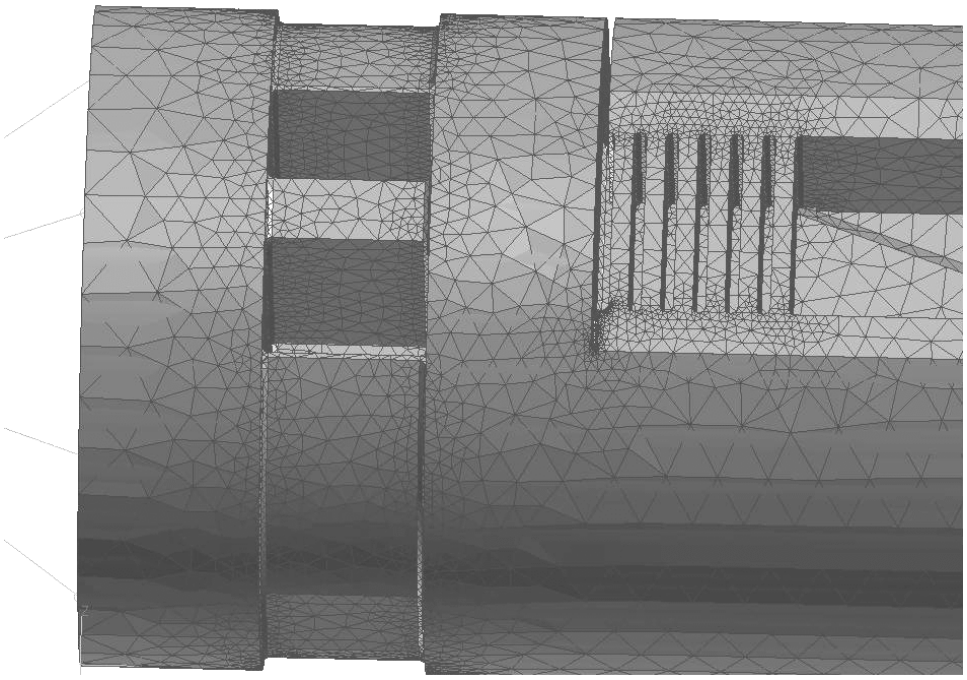

Figure 20. Closeup view: end of axial section.

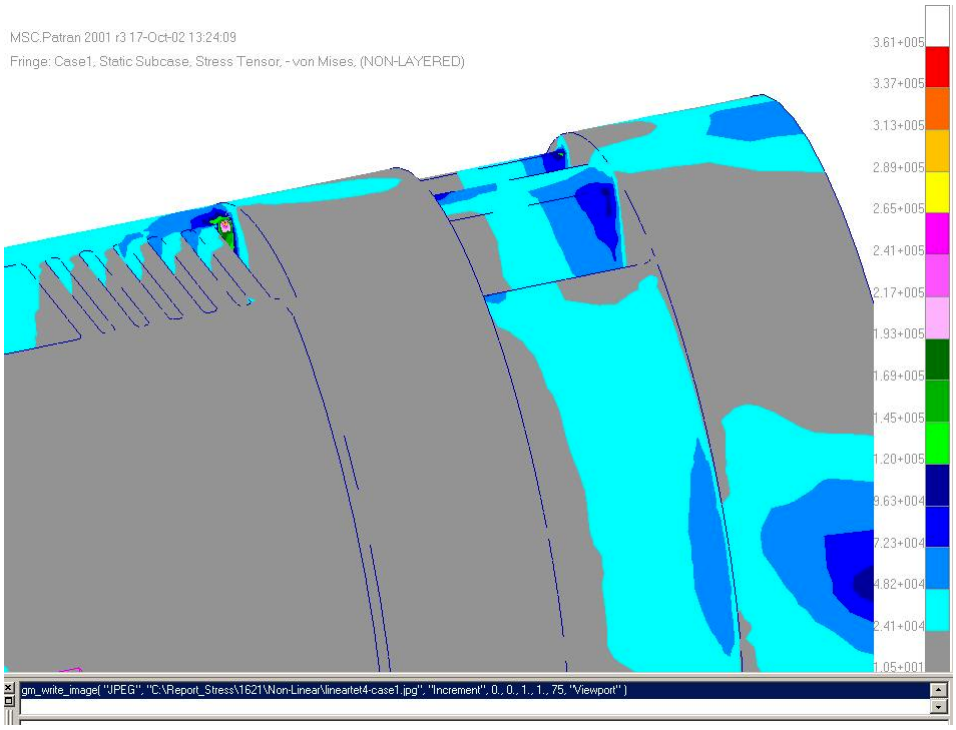

Figure 21. Von Mises stress for balance from linear analysis, load case 1.

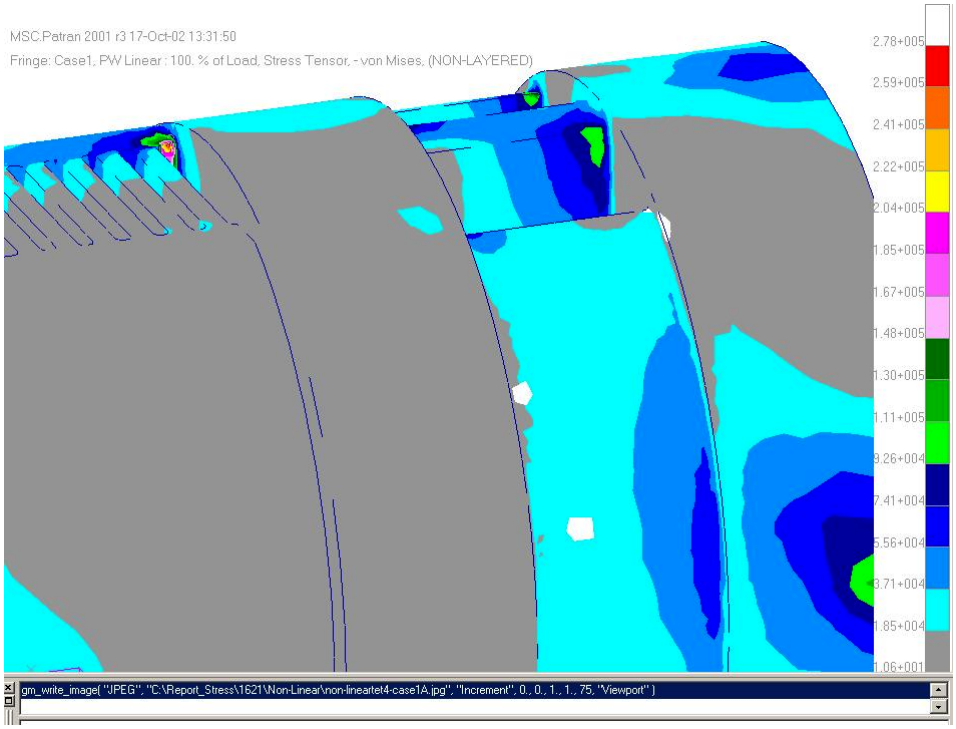

Figure 22. Von Mises stress for balance from nonlinear analysis, load case 1.

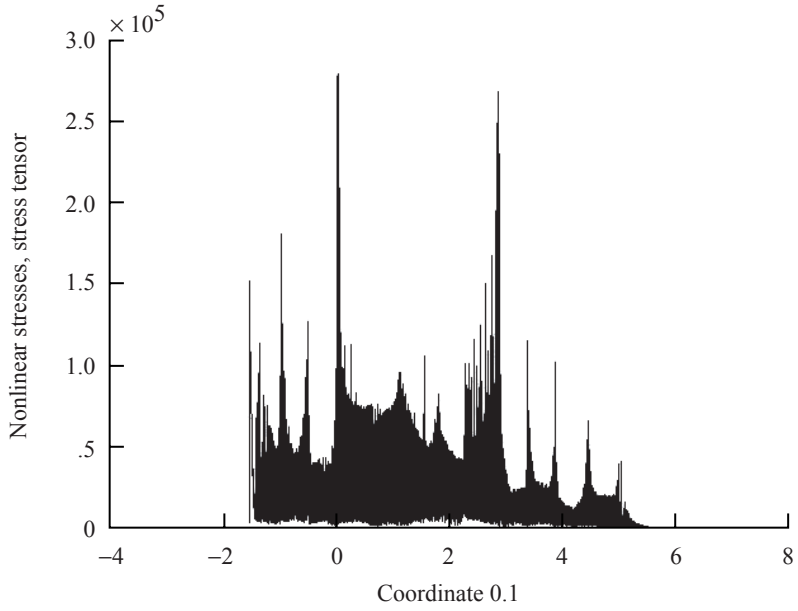

Figure 23. Axial position versus von Mises stress for all points on balance, load case 1.

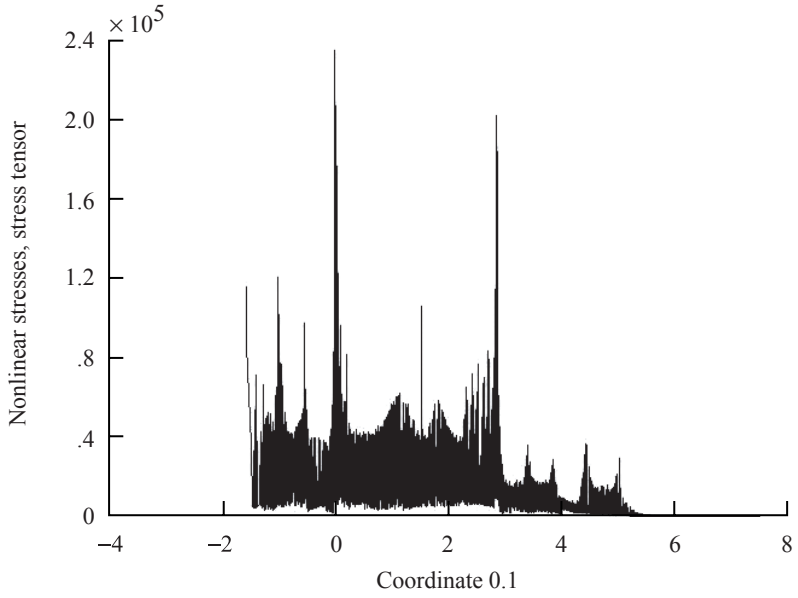

Figure 24. Position versus von Mises stress for points located on +Y side of balance, load case 1.

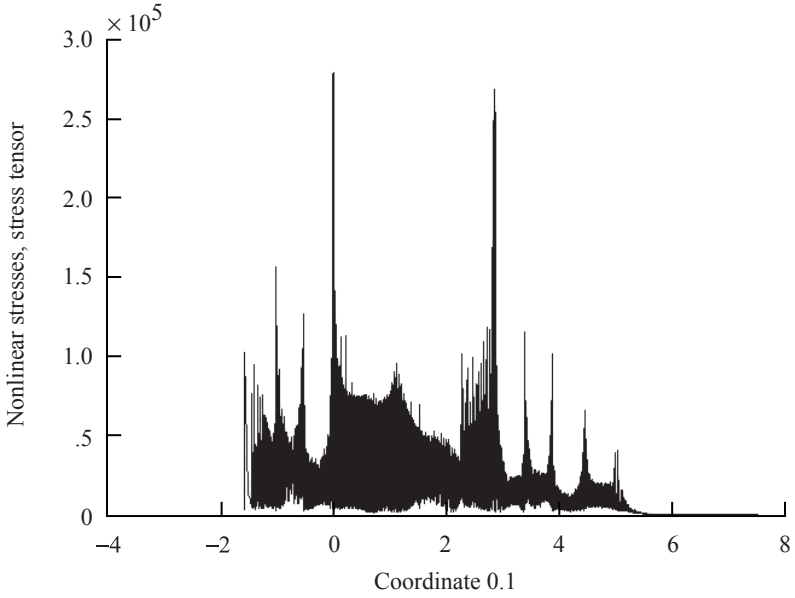

Figure 25. Position versus von Mises stress for points located on −Y side of balance, load case 1.

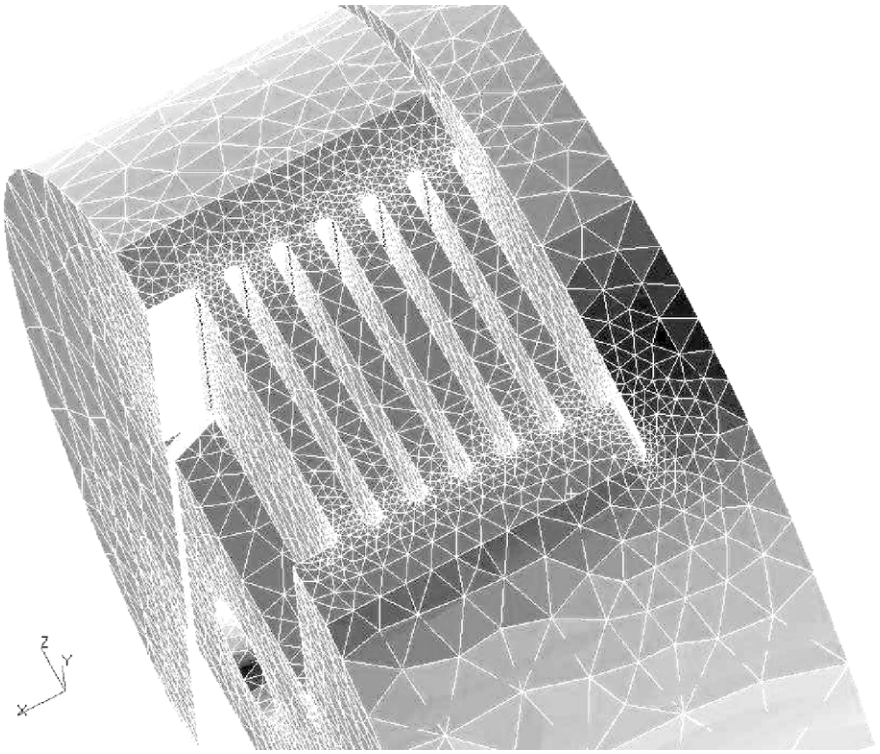

Figure 26. Axial section of balance near applied load.

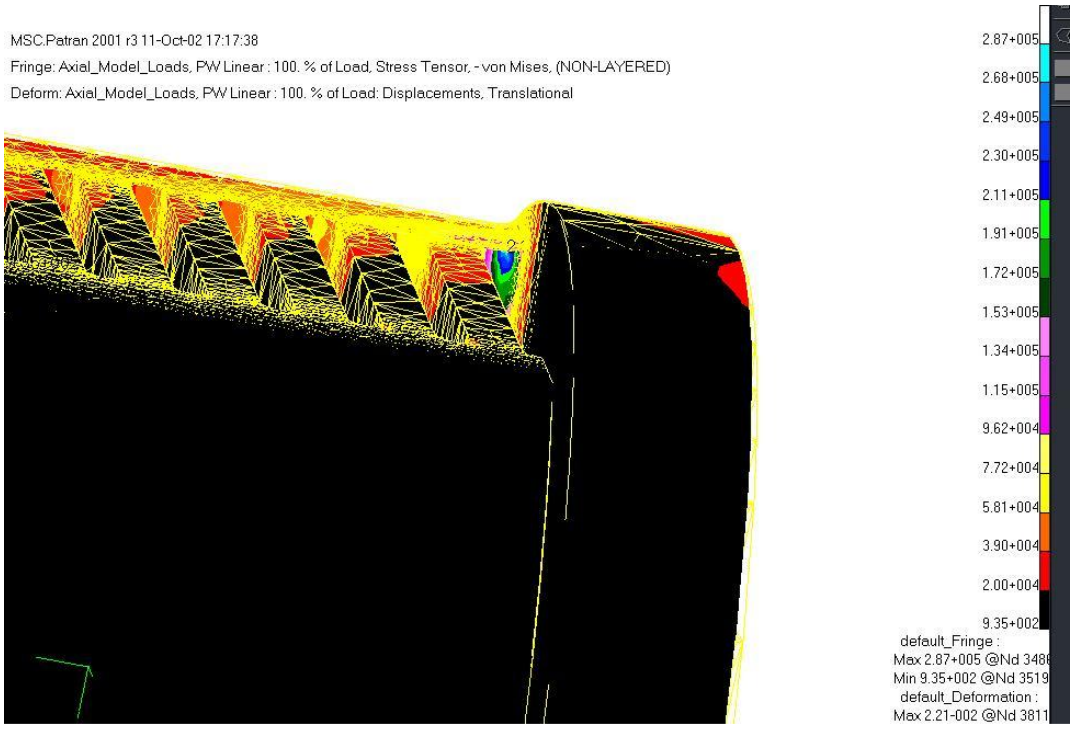

Figure 27. Von Mises stress for balance section near applied load from nonlinear analysis, load case 1.

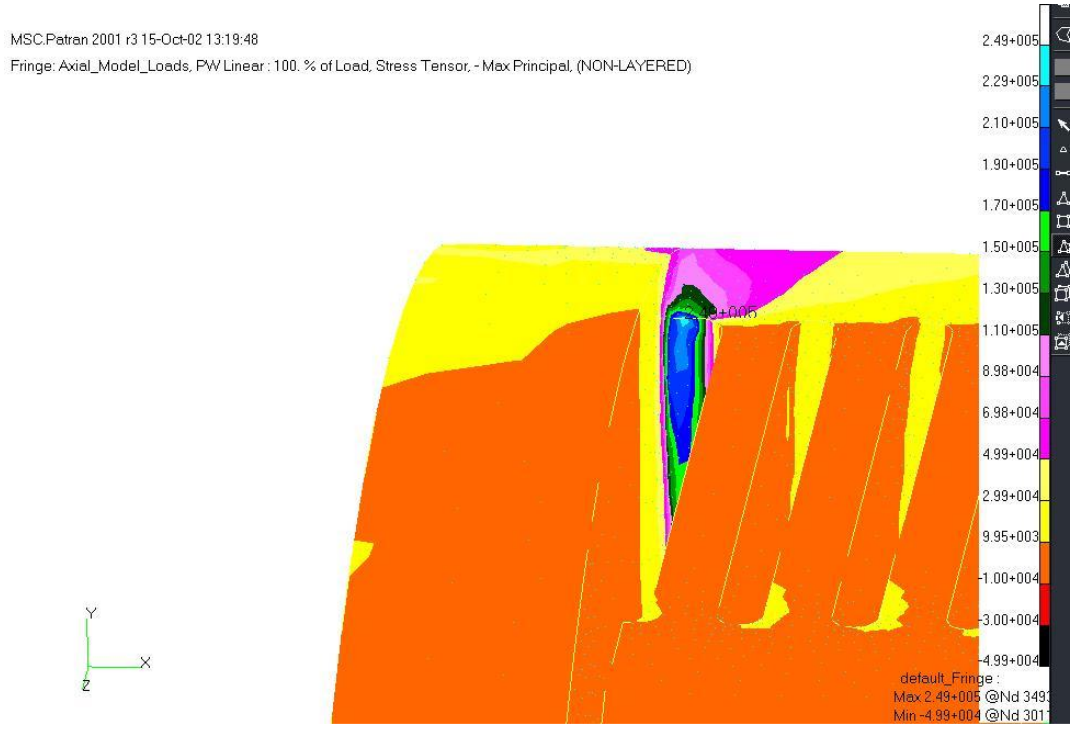

Figure 28. Principal stress for balance section near applied load from nonlinear analysis, load case 1.

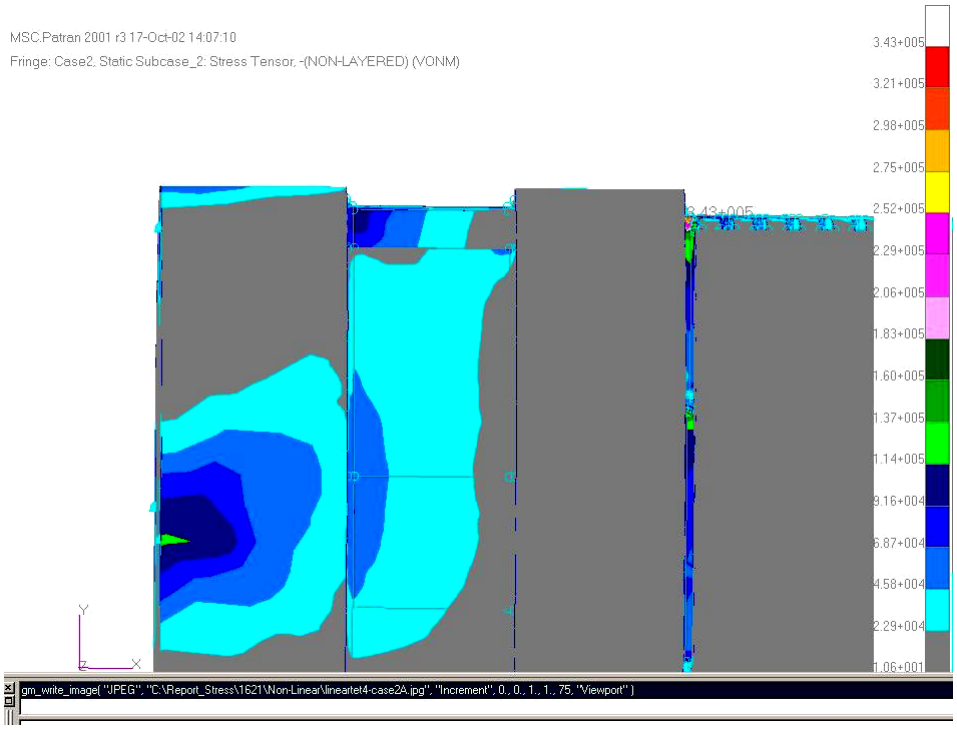

Figure 29. Von Mises stress for balance from linear analysis, load case 2.

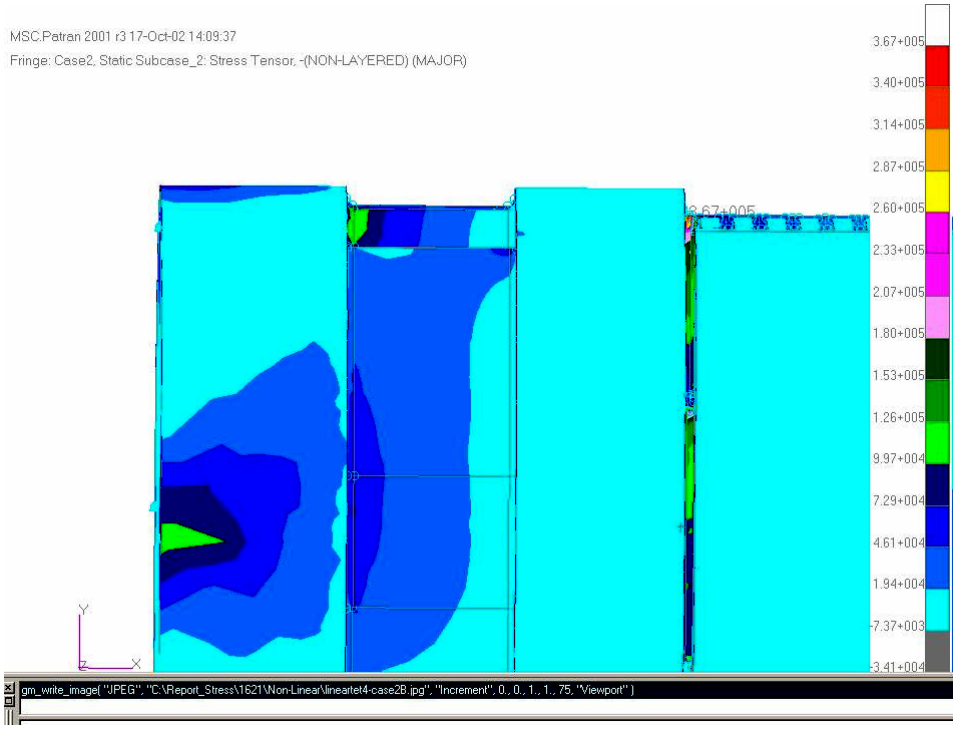

Figure 30. Principal stress for balance from linear analysis, load case 2.

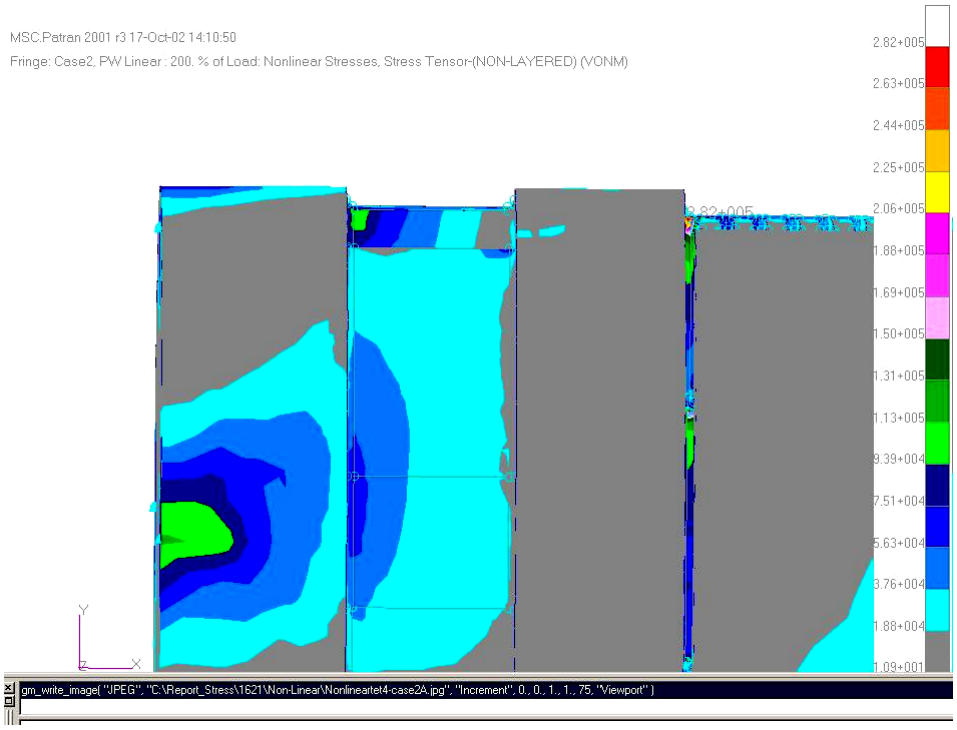

Figure 31. Von Mises stress for balance from nonlinear analysis, load case 2.

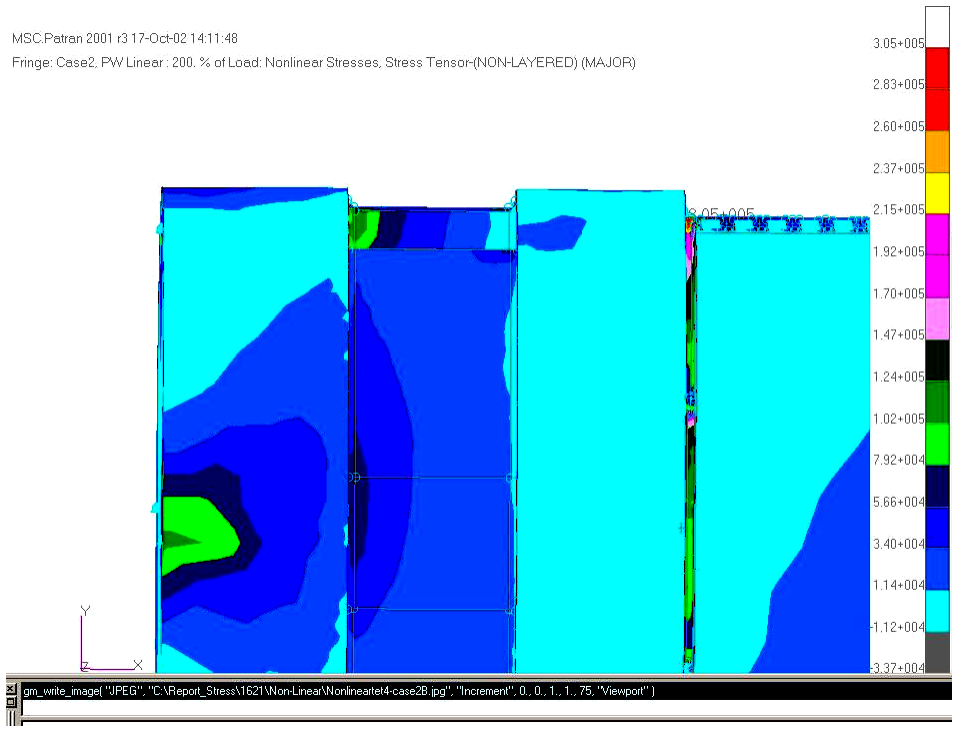

Figure 32. Principal stress for balance from nonlinear analysis, load case 2.

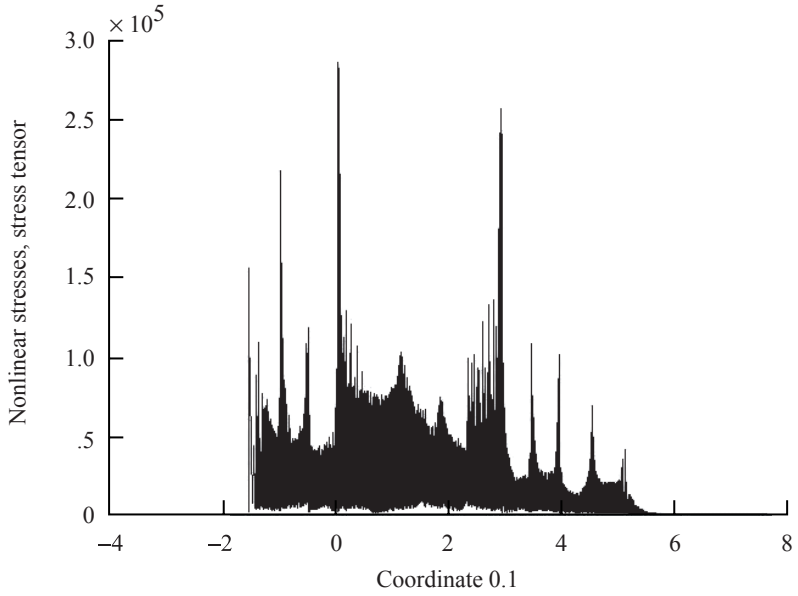

Figure 33. Position versus von Mises stress for all points on balance, load case 2.

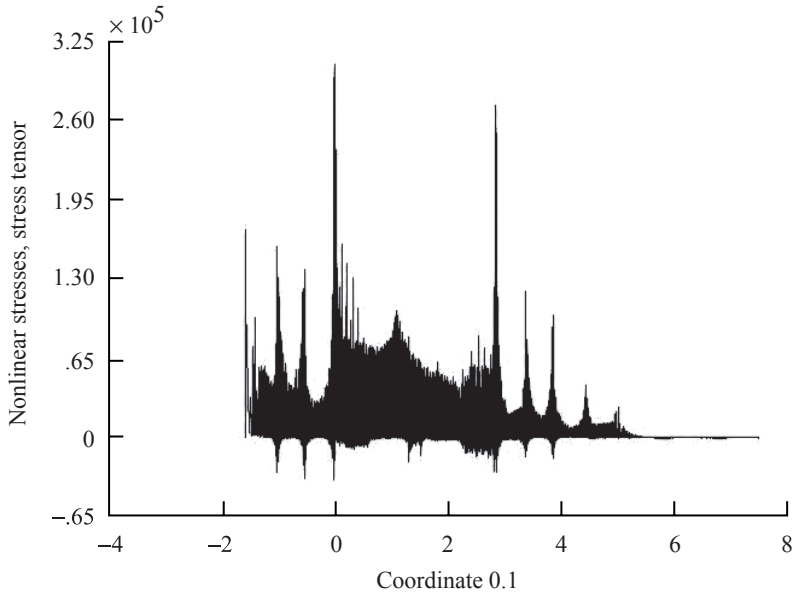

Figure 34. Position versus principal stress for all points on balance, load case 2.

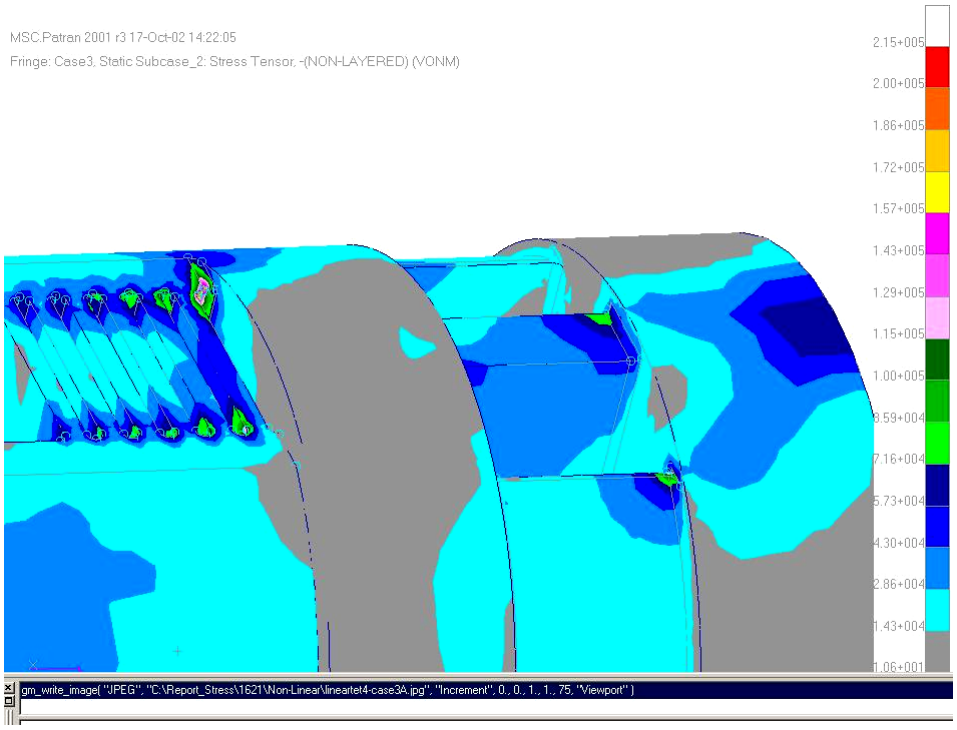

Figure 35. Von Mises stress for balance from linear analysis, load case 3.

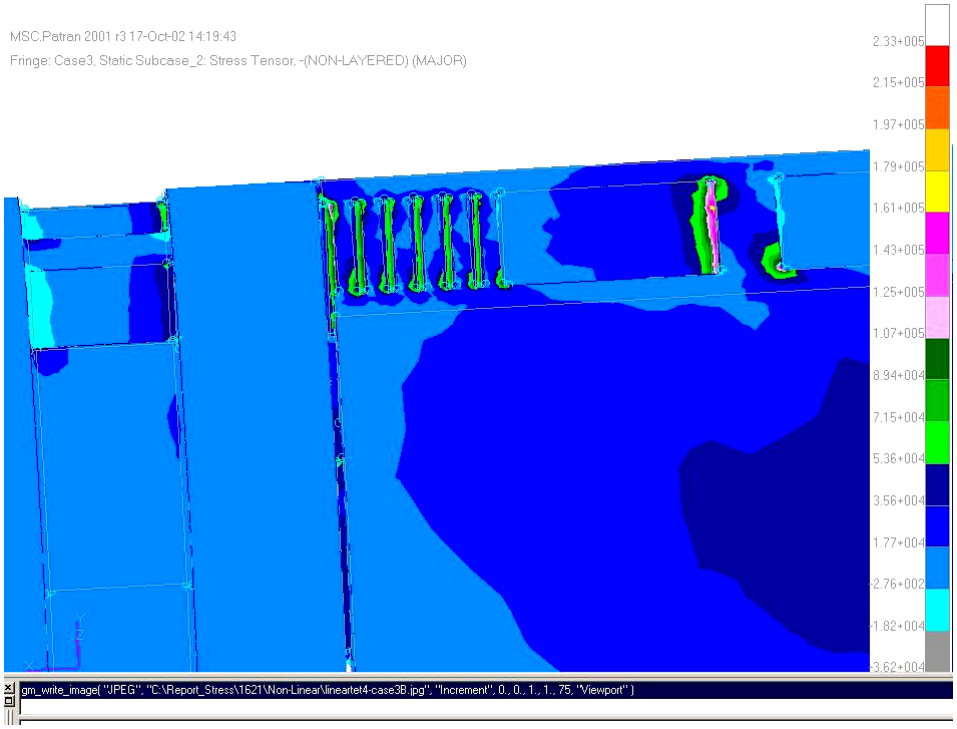

Figure 36. Principal stress for balance from linear analysis, load case 3.

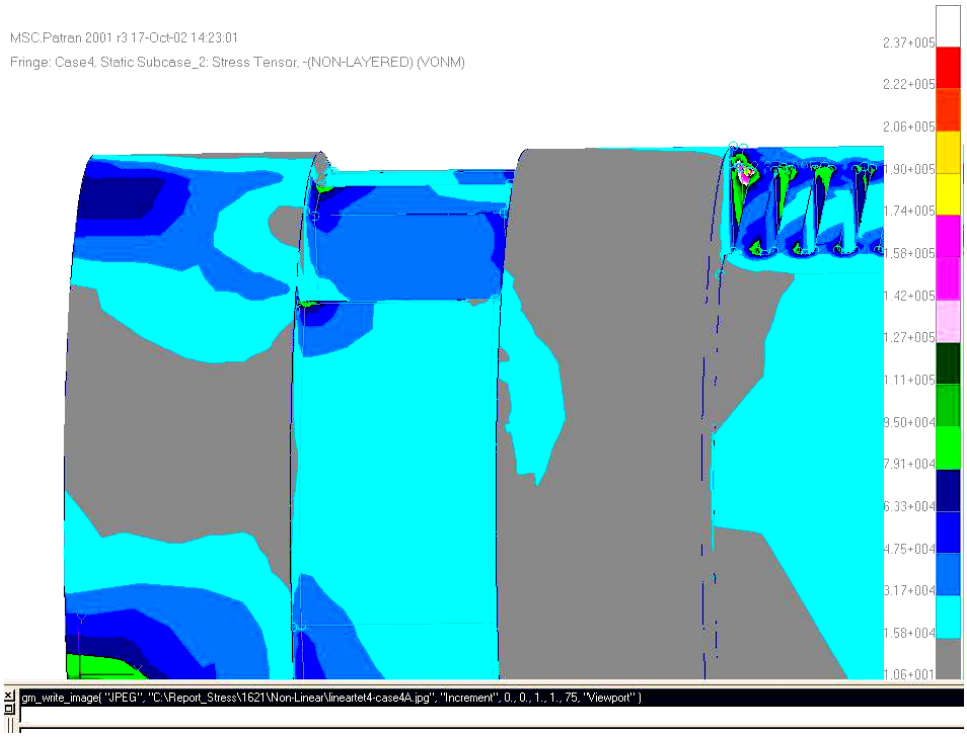

Figure 37. Von Mises stress for balance from linear analysis, load case 4.

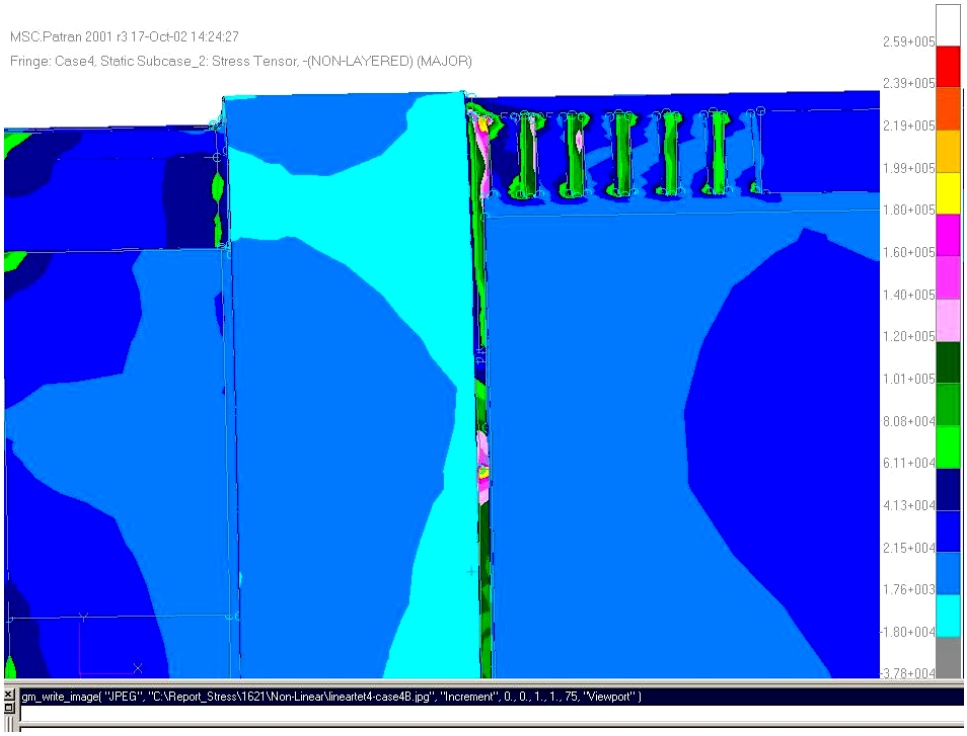

Figure 38. Principal stress for balance from linear analysis, load case 4.

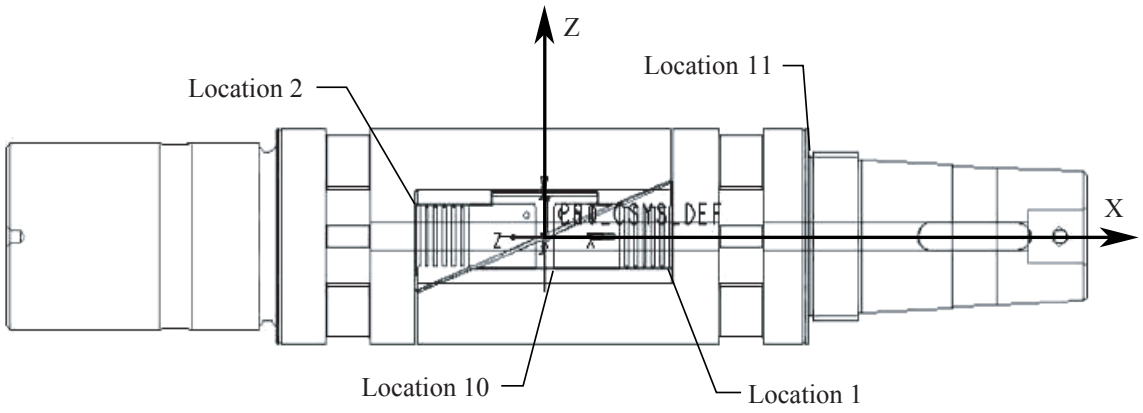

Figure 39. Balance 1621 with coordinate system and high stress region locations 1, 2, 10, and 11.

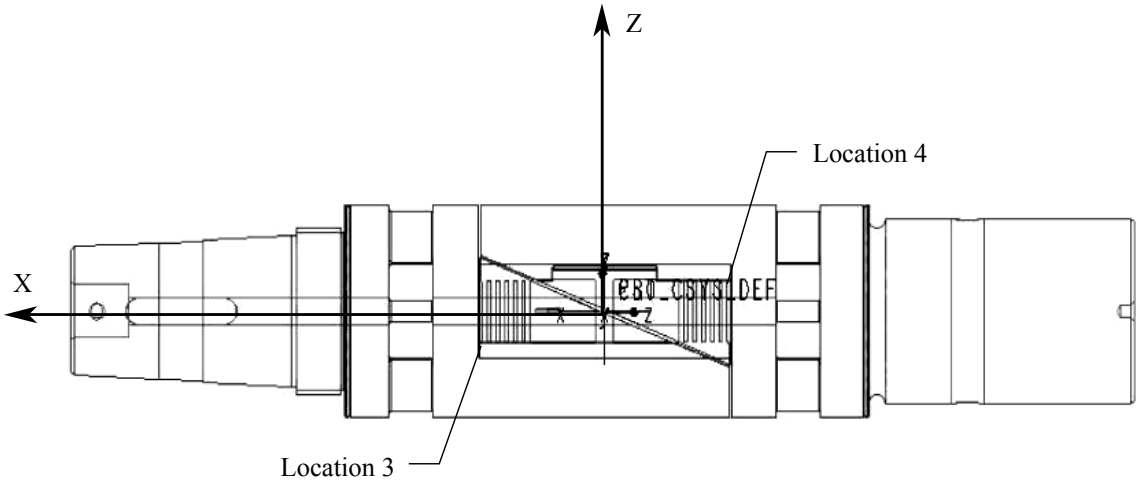

Figure 40. Balance 1621 with coordinate system and high stress region locations 3 and 4.

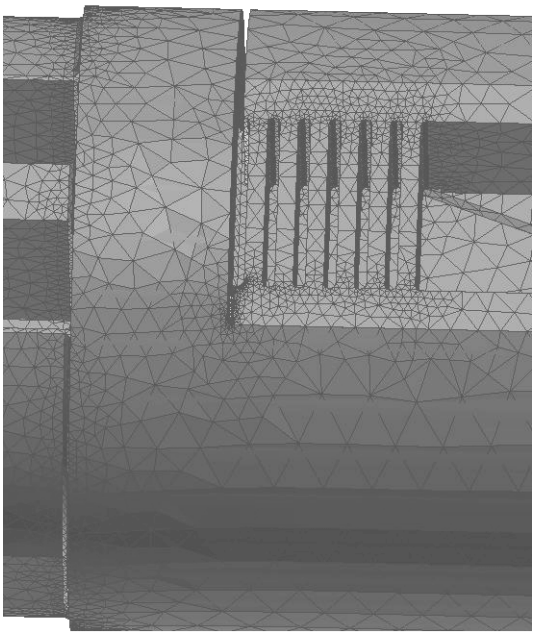

(a) Before modification.

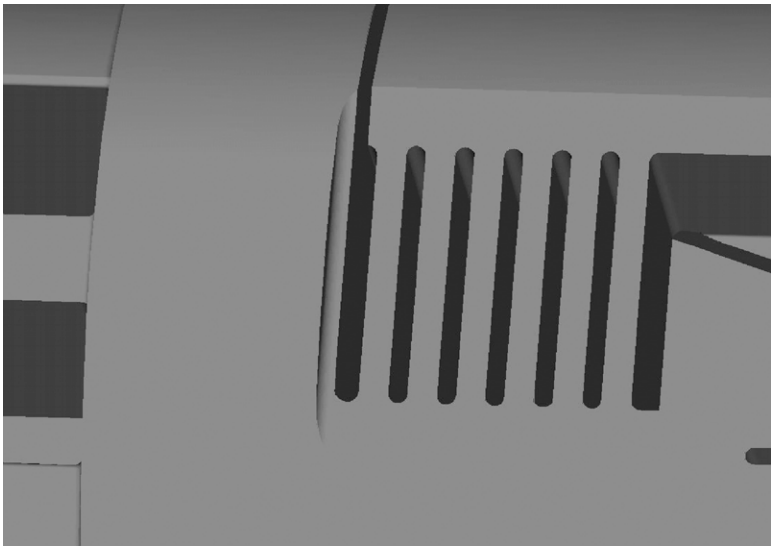

(b) After modification.

Figure 41. Closeup view of location 4 on balance 1621, model A.

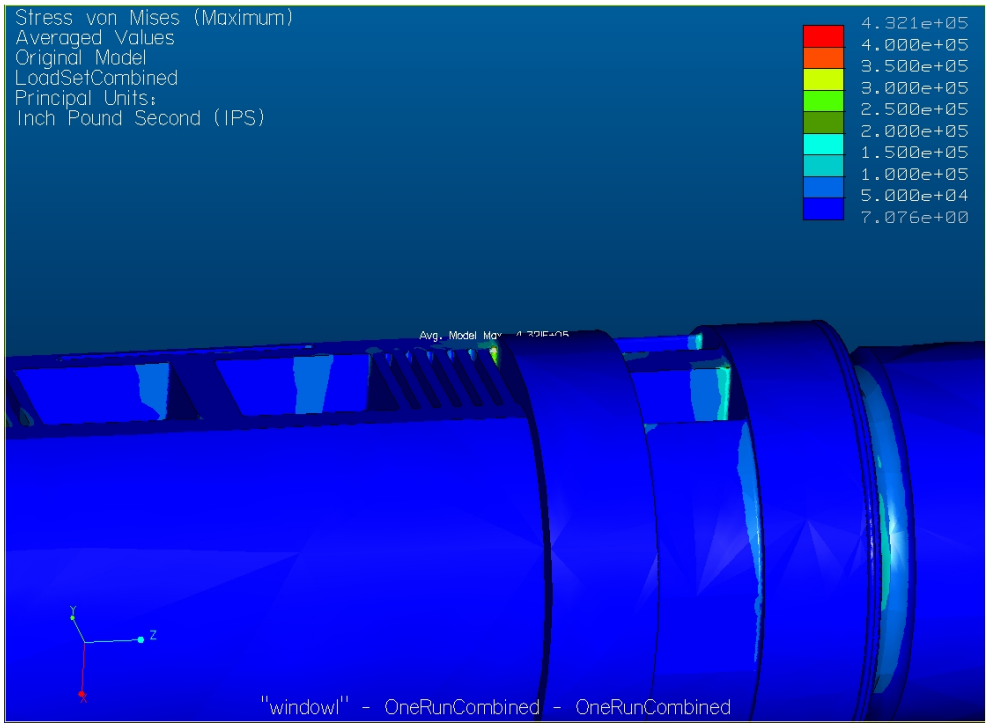

Figure 42. Maximum von Mises stress before modification using MPA.

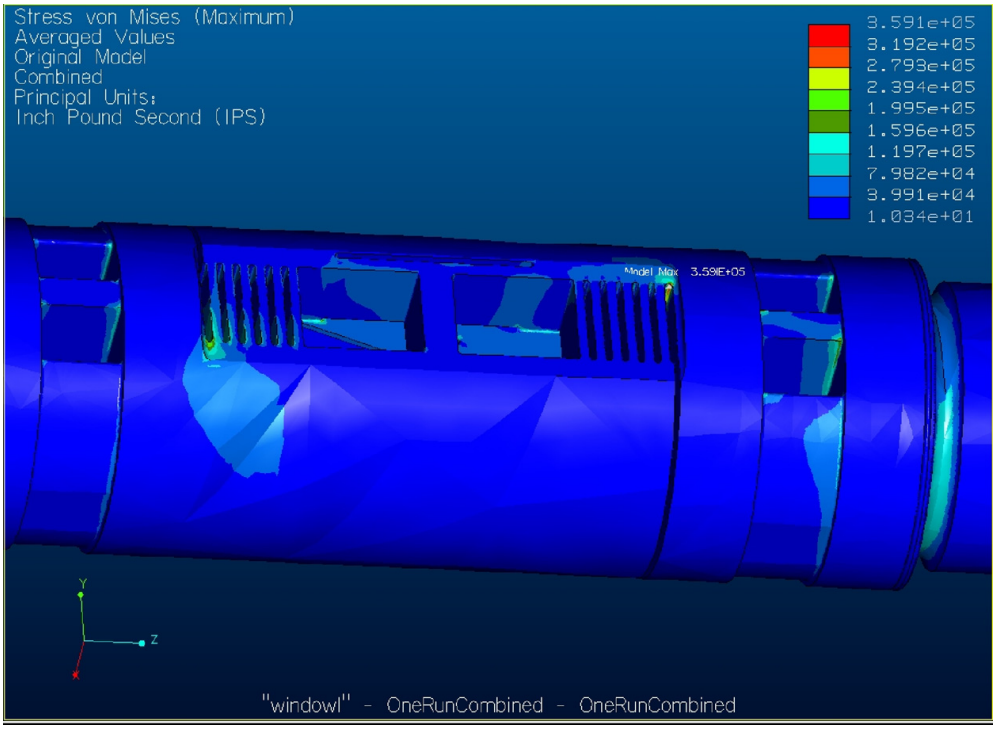

Figure 43. Maximum von Mises stress after modification using MPA.

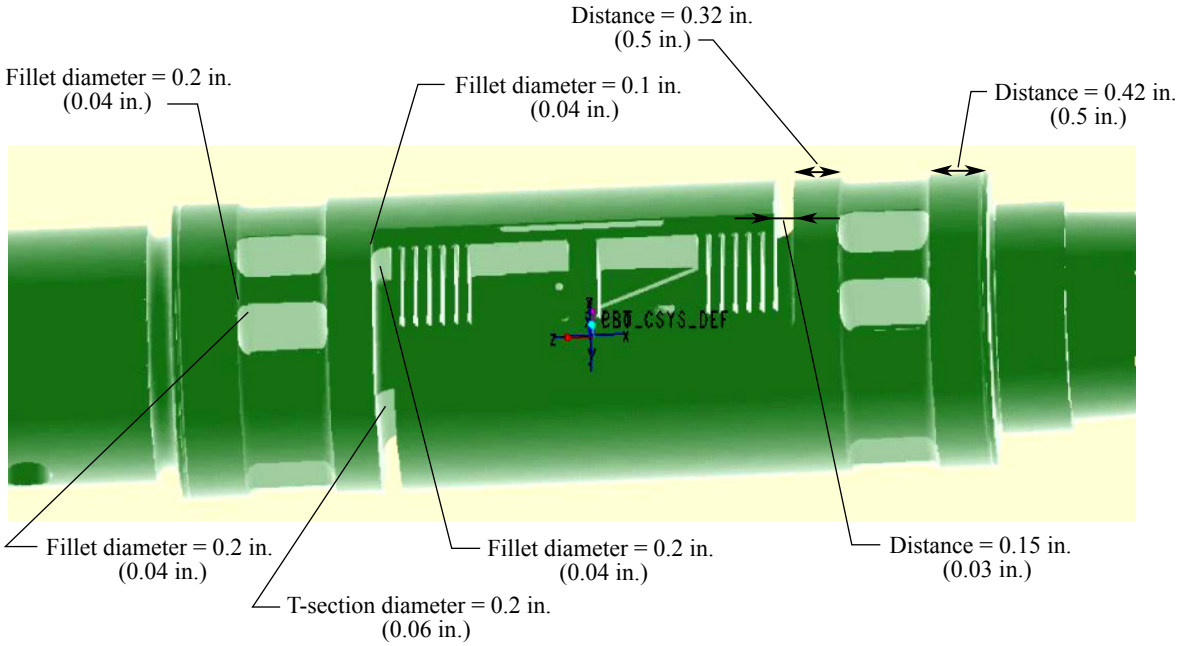

Figure 44. Balance 1621 after present modification, model B. Dimension before modification is shown in parentheses.

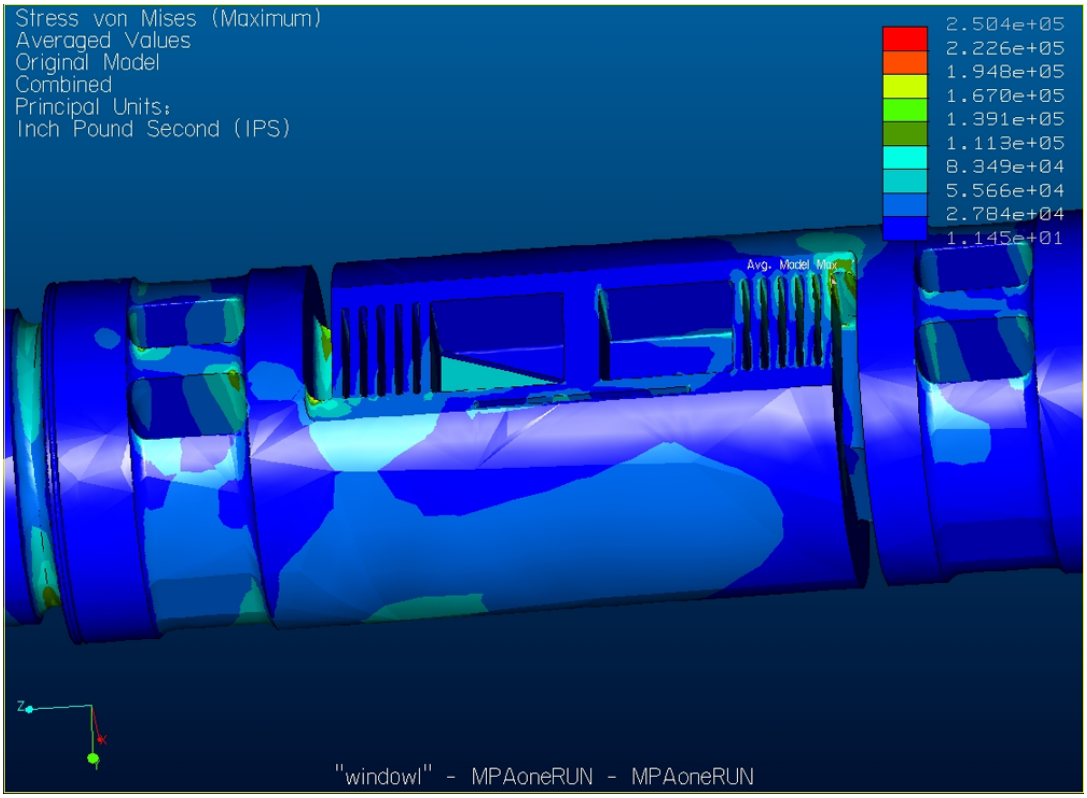

Figure 45. Maximum von Mises stress for model B using MPA.

REPORT DOCUMENTATION PAGE

Form Approved
OMB No. 0704-0188

1. REPORT DATE *(DD-MM-YYYY)*	2. REPORT TYPE	3. DATES COVERED *(From - To)*
01- 12 - 2004	Technical Memorandum	

4. TITLE AND SUBTITLE
Study and Analyses on the Structural Performance of a Balance

5a. CONTRACT NUMBER

5b. GRANT NUMBER

5c. PROGRAM ELEMENT NUMBER

6. AUTHOR(S)
Karkehabadi, R.; Rhew, R. D.; and Hope, D. J.

5d. PROJECT NUMBER

5e. TASK NUMBER

5f. WORK UNIT NUMBER
23-762-45-AE

7. PERFORMING ORGANIZATION NAME(S) AND ADDRESS(ES)
NASA Langley Research Center
Hampton, VA 23681-2199

8. PERFORMING ORGANIZATION REPORT NUMBER
L-18344

9. SPONSORING/MONITORING AGENCY NAME(S) AND ADDRESS(ES)
National Aeronautics and Space Administration
Washington, DC 20546-0001

10. SPONSOR/MONITOR'S ACRONYM(S)
NASA

11. SPONSOR/MONITOR'S REPORT NUMBER(S)
NASA/TM-2004-213263

12. DISTRIBUTION/AVAILABILITY STATEMENT
Unclassified - Unlimited
Subject Category 35
Availability: NASA CASI (301) 621-0390

13. SUPPLEMENTARY NOTES
Karkehabadi, Lockheed Martin, Hampton, VA. Rhew and Hope, Langley Research Center, Hampton, VA.
An electronic version can be found at http://techreports.larc.nasa.gov/ltrs/ or http://ntrs.nasa.gov

14. ABSTRACT

Strain-gauge balances for use in wind tunnels have been designed at Langley Research Center (LaRC) since its inception. Currently Langley has more than 300 balances available for its researchers. A force balance is inherently a critically stressed component due to the requirements of measurement sensitivity. The strain-gauge balances have been used in Langley's wind tunnels for a wide variety of aerodynamic tests, and the designs encompass a large array of sizes, loads, and environmental effects. As the emphasis increases on improving aerodynamic performance of all types of aircraft and spacecraft, the demand for improved balances is at the forefront. Force balance stress analysis and acceptance criteria are under review due to LaRC wind tunnel operational safety requirements. This paper presents some of the analyses and research done at LaRC that influence structural integrity of the balances. The analyses are helpful in understanding the overall behavior of existing balances and can be used in the design of new balances to enhance performance. Initially, a maximum load combination was used for a linear structural analysis. When nonlinear effects were encountered, the analysis was extended to include nonlinearities using MSC.Nastran™.

15. SUBJECT TERMS
Balance; Wind tunnel; Stress; Sharp corners; Linear analysis

16. SECURITY CLASSIFICATION OF:			17. LIMITATION OF ABSTRACT	18. NUMBER OF PAGES	19a. NAME OF RESPONSIBLE PERSON
a. REPORT	b. ABSTRACT	c. THIS PAGE			STI Help Desk (email: help@sti.nasa.gov)
					19b. TELEPHONE NUMBER *(Include area code)*
U	U	U	UU	39	(301) 621-0390